SPATIOTEMPORAL NONLINEAR DYNAMICS IN GRADED-INDEX MULTIMODE FIBERS

A THESIS SUBMITTED TO

THE GRADUATE SCHOOL OF ENGINEERING AND SCIENCE

OF BILKENT UNIVERSITY

IN PARTIAL FULFILLMENT OF THE REQUIREMENTS FOR

THE DEGREE OF

MASTER OF SCIENCE

IN

MATERIALS SCIENCE AND NANOTECHNOLOGY

By

Uğur Teğin

May 2018

SPATIOTEMPORAL NONLINEAR DYNAMICS IN GRADED-INDEX MULTIMODE FIBERS
By Uğur Teğin
May 2018

We certify that we have read this thesis and that in our opinion it is fully adequate, in scope and in quality, as a thesis for the degree of Master of Science.

Bülend Ortaç(Advisor)

Talip Serkan Kasırga

Barış Akaoğlu

Approved for the Graduate School of Engineering and Science:

Ezhan Karaşan
Director of the Graduate School

ABSTRACT

SPATIOTEMPORAL NONLINEAR DYNAMICS IN GRADED-INDEX MULTIMODE FIBERS

Uğur Teğin
M.S. in Materials Science and Nanotechnology
Advisor: Bülend Ortaç
May 2018

Spatiotemporal pulse propagation in multimode fibers is generally considered as chaotic. Graded-index multimode fibers reduce the complexity due to its equal spacing of the modal wave numbers which also introduces a periodic self-imaging to the propagating beam. This unique phenomenon affects the coupling between the modes thus graded-index multimode fibers are an ideal testbed to study spatiotemporal pulse propagation. In this thesis, various spatiotemporal nonlinear dynamics studied in graded-index multimode fibers to achieve wavelength conversion, supercontinuum generation triggered by cascaded Raman scattering and to develop a novel all-fiber all-normal dispersion mode-locked laser cavity.

In normal dispersion regime, spatiotemporal instability of femtosecond pulses discovered numerically and experimentally by exciting a graded-index multimode fiber with a Ti:Sapphire laser capable to generate 200 fs pulses at 800 nm. With 90 THz frequency shift, Stokes and anti-Stokes sidebands are observed. The signature of spatiotemporal instability which allows the sidebands to inherit the spatial distribution of the pump pulse is observed with the spatial characterization of the generated sidebands.

Later a high power laser system with adjustable output parameters is developed as a pump source for spatiotemporal nonlinear pulse propagation studies. By employing this source, with MHz pump pulse repetition rate high power octave-spanning supercontinuum generation triggered by cascaded Raman scattering is demonstrated. The results obtained with this novel method is the highest average power and repetition supercontinuum source with a standard graded-index multimode fiber in the literature.

Additional spatiotemporal wavelength conversion mechanisms, a small graded-index multimode fiber between single mode fiber segments can be used as a bandpass filter and saturable absorber. These effects are combined in an all-fiber all normal dispersion laser cavity for the first time in the literature. In the demonstrated cavity design, mode-locking is achieved by nonlinear multimodal interference in graded-index multimode fiber segment. All-normal cavity design supports dissipative soliton pulse formation but it requires bandpass filtering. This requirement is satisfied with multimode interference reimaging thus a unique and simple all-fiber cavity design is constructed to generate ultrashort dissipative soliton pulses. The developed oscillator generates 5 ps pulses at 1030 nm with 44 MHz repetition rate. These pulses are externally compressed to 276 fs. All-fiber cavity design ensures stability and 70 dB sideband suppression is measured in radio frequency domain.

Keywords: Fiber lasers, Graded-index multimode fibers, Ytterbium doped fibers, Nonlinear fiber optics, Spatiotemporal nonlinear dynamics.

ÖZET

KADEMELİ-İNDEKS ÇOK MODLU FİBERLERDE UZAYSAL-ZAMANSAL DOĞRUSAL OLMAYAN DİNAMİKLER

Uğur Teğin
Malzeme Bilimi ve Nanoteknoloji, Yüksek Lisans
Tez Danışmanı: Bülend Ortaç
Mayıs 2018

Uzaysal-zamansal atım ilerleyişi çok modlu fiberlerde genellikle kaotik olarak değerlendirilmiştir. Fiber içerisinde ilerleyen ışının periyodik öz-görüntülemeye maruz kalmasını sağlayan mod dalga sayılarının eş aralıklarla dizilmesi sonucunda kademeli-indeks çok modlu fiberlerde bu karışıklık daha azdır. Bu benzersiz olgu modlar arasında birleşmeyi de etkilediği için kademeli-indeks çok modlu fiberler uzaysal-zamansal atım ilerleyişi çalışmaları için ideal sınama ortamıdır. Bu tezde, kademeli-indeks çok modlu fiberlerde çeşitli uzaysal-zamansal doğrusal olmayan dinamikler çalışılarak dalgaboyu dönüştürme, kademeli Raman saçılımının tetiklediği süpersüreklilik oluşturma ve tamamen fiber ve tamamen normal yayılma düzeninde çalışan lazer kavitesi geliştirilmiştir.

Normal yayılma düzeninde 800 nm dalgaboyunda 200 fs atımlar üretebilen bir Ti:Safir lazeri ile femtosaniye atımların uzaysal-zamansal kararsızlığı nümerik ve deneysel olarak keşfetildi. 90 THz frekans kayması ile Stokes ve anti-Stokes yanbantları deneylerde gözlemlendi. Yanbantların pompa atımının uzaysal dağılımını devralmasını sağlayan uzaysal-zamansal kararsızlığın imzası yanbantlar için yapılan karakterizeler sırasında gözlemlendi.

Ardından ayarlanabilir çıkış özelliklerine sahip yüksek güçlü bir lazer sistemi uzaysal-zamansal doğrusal olmayan atım ilerleyişi çalışmaları için pompa kaynağı olarak geliştirildi. Bu kaynak lazeri kullanılarak kademeli Raman saçılımı ile başlayan MHz pompa atım tekrar oranında yüksek güçlü oktav-kaplayan süpersüreklilik oluşturulabildiği gösterildi. Bu özgün yöntem ile elde edilen sonuçlar literatürde kademeli-indeks çok modlu fiberler ile üretilen en yüksek güç ve tekrar oranına sahip süpersürekliliktir.

Uzaysal-zamansal dalgaboyu dönüştürme çalışmalarına ek olarak küçük bir kademeli-indeks çok modlu fiber parçasının tek modlu fiberlerin arasında kullanımı ile kuşak geçirici filtre ve doyurulabilir emici olarak kullanılabilir. Literatürde ilk defa bu etkiler bir tamamen fiber ve tamamen normal yayılma düzeninde çalışan lazer kavitesinde birleştirilmiştir. Geliştirilen lazer kavitesi tasarımında mod-kilitleme doğrusal olmayan çok modlu karışma ile elde edilmiştir. Tamamen fiber lazer kavitesi tasarımı dissipative soliton atım türünü desteklemektedir ama bunun için kuşak geçirici filtreye ihtiyaç duymaktadır. Bu ihtiyaç çok modlu karışma tekrar görüntüleme tekniği ile karşılanarak, ultrakısa dissipative soliton atımları üretmek için basit tamamen fiber bir lazer tasarımı kurulmuştur. Geliştirilen lazer 44 MHz tekrar oranıyla 1030 nm dalgaboyunda 5 ps süreli atımlar oluşturmaktadır. Bu atımlar haricen 276 fs süresine kadar sıkıştırılabilmektedir. Tamamen fiber kavite tasarımı kararlılığı sağladığı için radyo frekansı alanında 70 dB mertebesinde kenar bandı baskılama ölçülmüştür.

Anahtar sözcükler: Fiber lazerler, Kademeli-indeks çok modlu fibeler, İterbiyum katkılı fiberler, Doğrusal olmayan fiber optik, Uzaysal-zamansal doğrusal olmayan dinamikler .

Acknowledgement

I would like to thank my advisor Dr. Bülend Ortaç for his guidance and support during my study. Thanks to his patience and encouragement, I could find a chance to developed myself to conduct research.

I would like to thank to the recent and former members of Ortaç Research Group especially Bartu Şimşek,Yakup Midilli, Dr. Canan Kurşungöz, Dr. Tolga Bağcı, Levent Ersoy and Ahmet Başaran for their invaluable friendship and support.

I would like to thank my parents Abdullah Teğin and Keziban Teğin for their endless care and love. Their support and encourage lead me to science. I would like to thank my brothers Umut Teğin and Abitter Teğin for their endless support and counsel. I would also like to thank to my lovely fiancée, Ayşen Nur Akçay for her patience and endless love during this challenging period. Without her, all of this would not have been possible.

I would like to thank to Çağrı Şenel and Saniye Sinem Yılmaz for their priceless guidance, support and friendship. I am deeply indebted to them for their counsel since my undergraduate years.

Lastly, I would especially like to thank Akın Gün, Koray Yavuz, Abdüllatif Önen, Didem Dede, Denizhan Koray Kesim, Özgün Yavuz, Murat Serhatlıoğlu and Mohammad Asghari for their friendship and the great times that we shared.

Contents

List of Figures

Chapter 1

Introduction

Even though the total internal reflection is demonstrated in late 19th century, the theorization of low loss, silica glass modern fiber is presented in 1966 by Charles K. Kao and George A. Hockham [2, 3]. With the development of highly pure low loss optical glass fiber, modern optical fibers are started to used in communication technologies for data transferring with high bandwidths [4]. By doping optical glass fibers with rare-earth elements such as ytterbium, erbium, thulium and holmium, fiber based signal amplifiers and lasers are became attainable.

Due to high single-pass gain and alignment-free configurations, optical fiber based pulsed sources have attracted a great attention. In 1986 the first mode-locked fiber laser is demonstrated utilizing neodymium-doped fiber [5]. Nowadays, ytterbium and erbium based mode-locked fiber lasers became low cost and environmentally stable solutions to produce ultrashort pulses on the order of picoseconds and femtoseconds. By exploiting different nonlinear dynamics in single mode fibers researchers discovered various pulse types such as soliton, parabolic and dissipative soliton pulses [6, 7, 8, 9]. Later with photonic crystal fibers nonlinear fiber optics studied extensively since this innovation allowed researchers to tune fibers characteristic properties like dispersion and nonlinearity. Via engineered fibers coherent supercontinuum generation, watt-level femtosecond oscillators and many new possibilities are incorporated into fiber based technologies

[10, 11].

Nowadays, a lot of efforts in nonlinear fiber optics community transferred to understand spatiotemporal dynamics in multimode fibers. In these studies, Due to its relatively less chaoticity, graded-index multimode fibers (GIMFs) are selected as test medium. The light propagating in these fibers experiences periodic self-imaging because of equal spacing of modal wave numbers. This unique way of propagation enables strong nonlinear coupling among the modes. Regarding the selection of pump pulse excites the GIMF dispersive wave generation, cascaded Raman scattering, multimode fiber multimode solitons, self-beam cleaning, harmonic generation and spatiotemporal instability is discovered very recently [12, 13, 14, 15, 16, 17].

In this thesis, picosecond and femtosecond nonlinear pulse propagation is studied in GIMFs. First, a titanium-sapphire based commercial solid state laser capable to generate 200 fs pulses in normal dispersion regime is preferred to excite GIMFs. The outcome of this study, spatiotemporal instability of femtosecond pulses are observed first time in the literature both numerically and experimentally [18]. Experimentally observed spatiotemporal instability sidebands are 91 THz detuned from the pump wavelength, 800 nm. Detailed analysis carried out numerically by employing coupled-mode pulse propagation model. Numerically obtained results are well-aligned with experimental observations. Spatial evolution of the total field and spatiotemporal instability sidebands are calculated numerically and for input pulses of 200-fs duration, formation and evolution of spatiotemporal instability are shown in both spatial and temporal domains. Our results present the unique features of spatiotemporal instability such as remarkable frequency shift with the inherited beam shape of instability sidebands.

In the second part of this thesis, a home-made fiber laser system is developed to have freedom to study pump pulse parameters such as pulse duration and peak powers. By using this laser system as source for our studies, cascaded-Raman scattering based supercontinuum generation in GIMFs is first time in the literature [19]. Formation dynamics of supercontinua are investigated by studying the effect of fiber length and core size. High power handling capacity of the GIMFs is demonstrated by power scaling experiments. Pump pulse repetition rate is scaled from kHz to MHz while pump pulse peak power remains same and ∼4 W supercontinuum is achieved with 2 MHz pump repetition rate. To the best of our knowledge, this is the highest average power and repetition supercontinuum source ever reported based on a standard GIMF. Spatial properties of the generated supercontinua are measured and Gaussian-like beam profiles obtained for different wavelength ranges. Numerical simulations are performed to investigate underlying nonlinear dynamics in details and well-aligned with experimental observations.

Finally, a short GIMF segment is used in an all-fiber laser cavity to generate femtosecond pulses. Multimode interference employed to achieve spectral bandpass filtering and saturable absorption. By employing these effects an ytterbium based all-fiber mode-locked laser is introduced first time in the literature [20]. The introduced simple cavity generates dissipative soliton pulses at 1030 nm with 5.8 mW average power, 5 ps duration and 44.25 MHz repetition rate. Pulses are later dechirped to 276 fs via an external grating pair. All-fiber cavity design ensures high stability and 70 dB sideband suppression is obtained in the radio frequency spectrum.

Chapter 2

Theoretical Background

In this chapter, pulse propagation dynamics in single mode and multimode fibers are introduced. Numerical methods for both waveguide structures are demonstrated in details. Finally, mode-locked fiber lasers and main types will be described.

2.1 Pulse Propagation in Single Mode Fibers

2.1.1 Dispersion

Pulse propagating inside waveguide experiences dispersion and nonlinearity. The phase velocity of a wave depends on frequency and propagation mode. This dependency results in dispersion phenomenon. Most of all material dispersion which is also referred as chromatic dispersion plays a significant role in wave propagation. The chromatic dispersion is caused by frequency dependence of refractive index of the material. In optical waveguides such as fibers short pulse experiences chromatic dispersion since spectrum of a picosecond or femtosecond pulses are relatively broad. Effect of fiber dispersion commonly analyzed by using Taylor expansion to mode-propagation constant β about the frequency ω_0 where

ω_0 is the central frequency of the pulse.

$$\beta(\omega) = n(\omega)\frac{\omega}{c} = \beta_0 + \beta_1(\omega - \omega_0) + \frac{1}{2}\beta_2(\omega - \omega_0)^2 + ... \tag{2.1}$$

where β_m is defined as it follows.

$$\beta_m = \left(\frac{d^m\beta}{d\omega^m}\right)_{\omega=\omega_0} \tag{2.2}$$

Here β_2 is called as the group-velocity dispersion (GVD) coefficient. Especially in fiber communication community, one can also use dispersion parameter D to express fibers parameter.

$$D = -\frac{2\pi c}{\lambda^2}\beta_2 = \frac{-\lambda}{c}\frac{d^2n}{d\lambda^2} \tag{2.3}$$

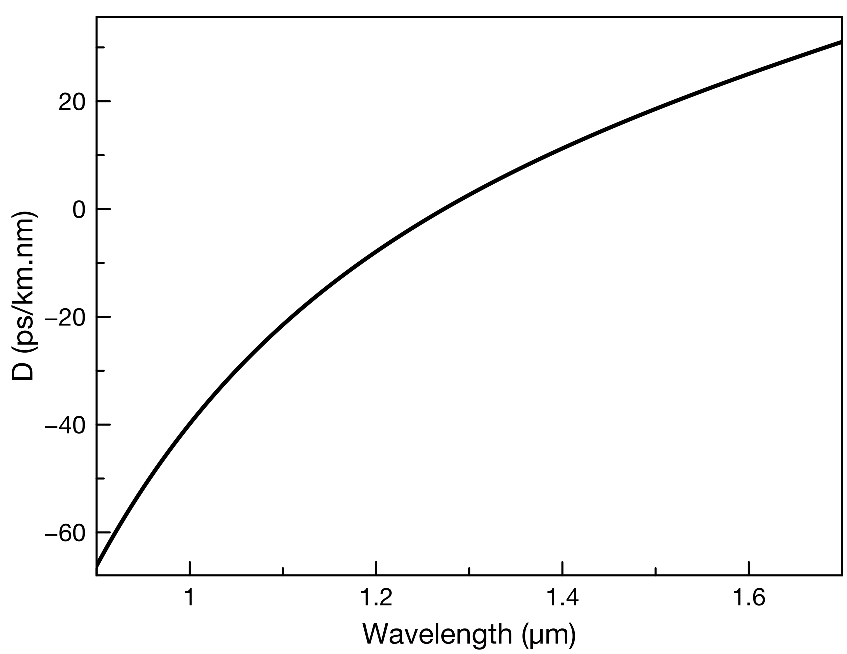

Figure 2.1: Variation of dispersion parameter (D) versus the wavelength for fused silica.

To calculate the aforementioned fiber dispersion parameters one need to obtain fibers refractive index which can be calculated by Sellmeier equation for fused silica (2.4) and the resulting refractive index is presented in Fig. 2.2 [21].

$$n(\lambda) = \sqrt{1 + \frac{0.6961663\lambda^2}{\lambda^2 - (0.0684043)^2} + \frac{0.4079426\lambda^2}{\lambda^2 - (0.1162414)^2} + \frac{0.8974794\lambda^2}{\lambda^2 - (9.896161)^2}} \quad (2.4)$$

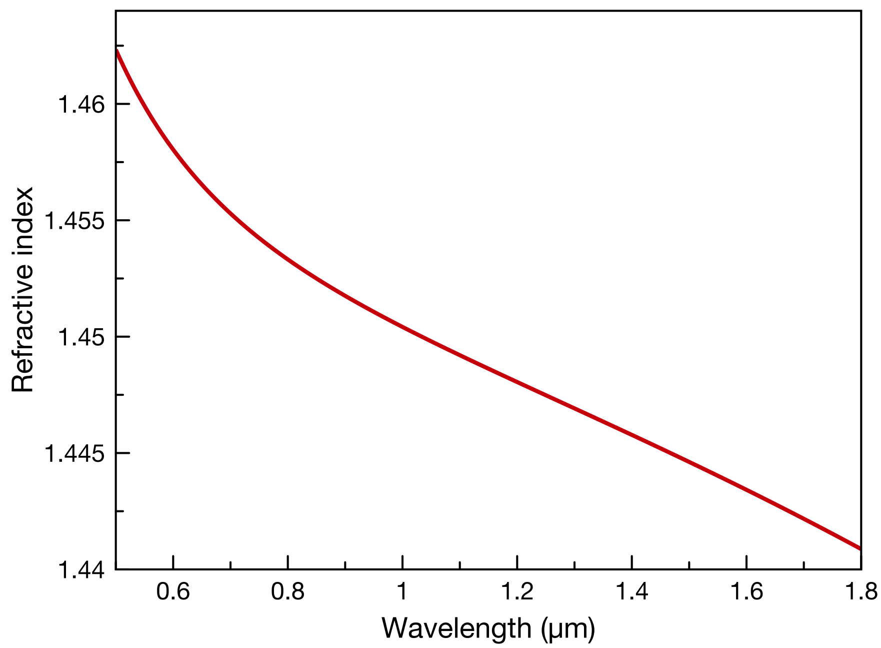

Figure 2.2: Variation of refractive index parameter (n) versus the wavelength for fused silica.

2.1.2 Fiber Nonlinearities

The response of the optical waveguide is nonlinear as a result of anharmonic motion of bound electrons in consequence to an applied field. For a short pulse Kerr effect and Raman scattering is dominant nonlinearities. The Kerr effect is a result of the dependence of the index of refraction to the intensity of the propagating wave:

$$n(I) = n_0 + n_2(I) \tag{2.5}$$

The Kerr coefficient of fused silica (n_2) is wavelength dependent and at 1 μm it is $2.7x10^{-20} m^2/W$ [1]. In the literature nonlinearity coefficient of the fiber is given as:

$$\gamma(\omega) = \frac{\omega n_2(\omega)}{c A_{eff}(\omega)} \tag{2.6}$$

where $A_{eff}(\omega)$ is the fibers effective mode area. The Kerr effect leads to various attractive nonlinear effects such as self-phase modulation and cross-phase modulation [1]. A beam experiences self-induced nonlinear phase shift during its propagation in optical fiber and its called self-phase modulation. This nonlinear phase shift can be also introduced by another beam propagating with different wavelength thus each propagating beam generates phase delay on other and this phenomenon called as cross-phase modulation.

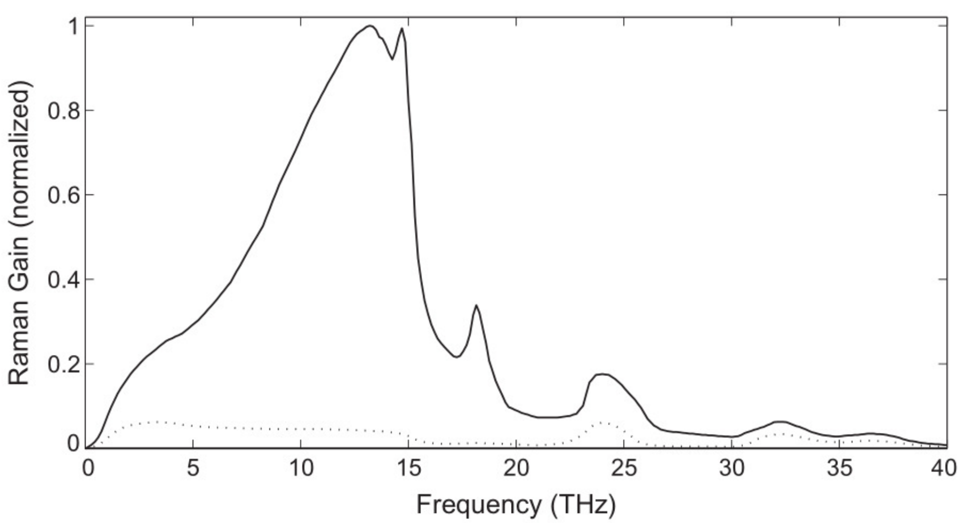

Figure 2.3: Raman gain (normalized) for silica fiber. When pump and Stokes wave are copolarized (orthogonally polarized) showed as solid (dotted) curve [1].

The optical field can transfer part of its energy to nonlinear medium via stimulated inelastic scattering such as stimulated Raman scattering (SRS) and stimulated Brillouin scattering (SBS) [22, 23]. Among these scatterings SBS is common for narrow-line lasers such as continuous-wave or single-frequency lasers and SRS is more common for the pulsed systems. SRS gain profile for the fused silica is presented in Fig. 2.3. SRS process can be used as a wavelength conversion method in fibers and short pulses can be generated at the outside of the bandwidth of gain-fibers. With this motivation Raman fiber amplifiers and fiber lasers are extensively studied in the literature [24, 25, 26].

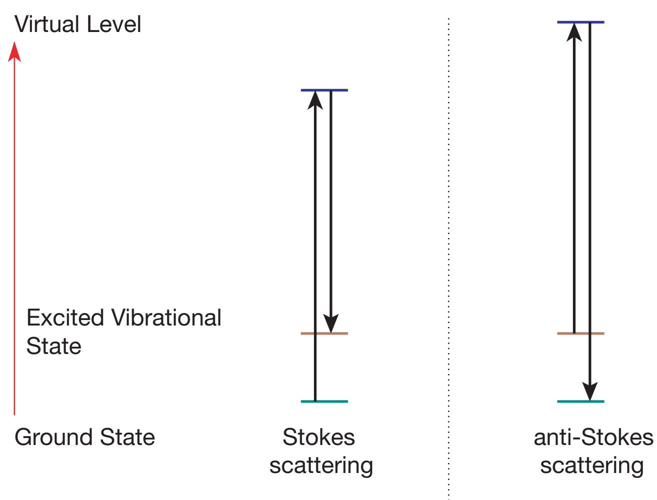

Figure 2.4: Quantum mechahical illustration of Raman Stokes and anti-Stokes scattering.

2.1.3 Nonlinear Schrödinger Equation

Evolution of the propagating optical fields envelope inside an optical fiber can be simply considered with GVD and nonlinearity coefficients as nonlinear Schrödinger equation (NLSE) expresses (Eq. (2.7)). With NLSE, pulse propagation on the z direction is studied in its simplest form and it is adequate to study continuous wave input and long pulses with low peak powers.

$$\frac{\partial A}{\partial z} = -i\frac{\beta_2}{2}\frac{\partial^2 A}{\partial T^2} + i\gamma \left|A\right|^2 A \tag{2.7}$$

Here A is the pulse amplitude normalized to obtain $\left|A\right|^2$ in terms of optical power. One can notice that the propagation is defined in retarded frame T. With the transformation defined in Eq. (2.8), the reference frame is moving with the pulse at group velocity v_g.

$$T = t - z/v_g \equiv t - \beta_1 z \tag{2.8}$$

For pulses of width $T_0 < 5$ps to obtain accurate results, one can generalize NLSE by considering higher-order dispersions ($\beta_3, \beta_4, \beta_5$), loss (or gain) coefficient, SRS and self-steepening terms. With these considerations generalized nonlinear Schrödinger equation (GNLSE) emerges (Eq.(2.9)). By numerically solving GNLSE, sufficiently correct results can be obtained for nonlinear processes such as supercontinuum generation.

$$\begin{aligned} &\frac{\partial A}{\partial z} + \frac{a}{2}A + \left(\sum_{n\geq 2}\beta_n \frac{i^{n-1}}{n!}\frac{\partial^n}{\partial t^n}\right) A = i\gamma\left(1 + \frac{\partial}{\partial t}\right) \\ &\times \left((1 - f_R)A\left|A\right|^2 + f_R A \int_0^\infty h_R(t')\left|A(z, t - t')\right|^2\right) \end{aligned} \tag{2.9}$$

In GNLSE, SRS can be included with introducing a response function [1]. Here f_R is the fractional contribution of the Raman effect and h_R is the delayed Raman response function.

2.1.4 Numerical Modeling of Single Mode Pulse Propagation in Optical Fibers

Various numerical methods introduced to solve NLSE and GNLSE for optical pulses longer than one optical cycle in the literature. These methods handle linear and nonlinear terms separately and heavily depends on fast Fourier transform since the derivations of the linear terms can be applied in frequency domain with less computational effort.

The most popular and straightforward numerical model to study NLSE and GLNSE is split-step Fourier method (SSFM) [1]. The motivation of this model is separation of the dispersion and nonlinear terms as

$$\frac{dA}{dz} = (\hat{D} + \hat{N})A \tag{2.10}$$

where $\hat{N}$ is the operator contains nonlinear terms and $\hat{D}$ is the operator contains dispersion, gain and loss terms. For GNLSE these terms are defined as follows and one can easily simplify these operators for NLSE.

$$\hat{N} = i\gamma \frac{1}{A}\left(1 + \frac{\partial}{\partial t}\right)\left((1 - f_R)A\left|A\right|^2 + f_R A \int_0^{\infty} h_R(t')\left|A(z, t - t')\right|^2\right) \tag{2.11}$$

$$\hat{D} = -\frac{a}{2} - \left(\sum_{n \geq 2} \beta_n \frac{i^{n-1}}{n!}\frac{\partial^n}{\partial t^n}\right) \tag{2.12}$$

The fundamental assumption of the SSFM is applying dispersion and nonlinearity operators separately for small propagation steps.

$$A(z + h, T) \approx exp(h\hat{D})exp(h\hat{N})A(z, T) \tag{2.13}$$

To apply dispersion operator to the Fourier transformed field, the dispersion operators each $\partial/\partial T$ term should be replaced with $-i\omega$ where ω the concerned frequency in Fourier domain [1]. In the most basic implementation method, the propagation from z to $z + h$ requires following steps.

$$
\begin{aligned}
A_1 &= exp(\hat{N}h/2)A(z,T) \\
A_2 &= exp(\hat{D}h/2)fft(A_1) \\
A(z+h,T) &= ifft(A_2)
\end{aligned}
\tag{2.14}
$$

The SSFM algorithm can be improved with the diagram presented in Fig. 2.5 which is also called as symmetrized SSFM. The symmetrized SSFM provides better accuracy but introduces additional calculation step to the propagation from z to $z+h$.

$$
A(z+h,T) \approx exp(\frac{h}{2}\hat{D})exp(\int_z^{z+h}\hat{N}(z')dz')exp(\frac{h}{2}\hat{D})A(z,T) \tag{2.15}
$$

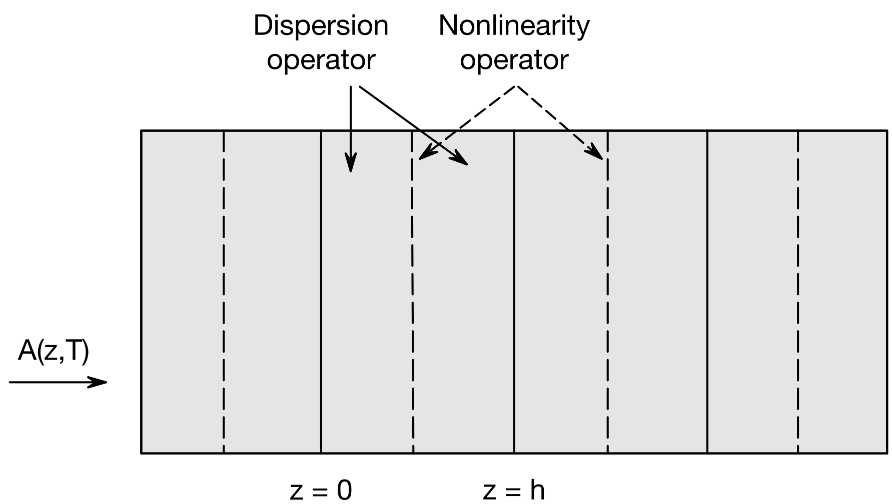

Figure 2.5: Illustration of the symmetrized split-step Fourier method.

In supercontinuum generation studies with photonic crystal fibers researchers developed more advanced models to simulate single-mode pulse propagation. Dudley at al. modified the GNLSE to solve it as a differential equation with a pre-build solvers [27]. Hult introduced fourth-order Runge-Kutta in the interaction picture method (RK4IP) which was developed to study Gross-Pitaevskii equation to fiber optics [28]. The RK4IP is more accurate than SSFM and its symmetrized version but the required steps to evalutate pulse propagation from z to $z+h$ as it follows,

$$\begin{aligned}
A_I &= exp(\frac{h}{2}\hat{D})A(z,T) \\
k_1 &= exp(\frac{h}{2}\hat{D})[h\hat{N}(A(z,T)]A(z,T) \\
k_2 &= h\hat{N}(A_I + k_1/2)[A_I + k_1/2] \\
k_3 &= h\hat{N}(A_I + k_2/2)[A_I + k_2/2] \\
k_4 &= h\hat{N}(exp(\frac{h}{2}\hat{D})(A_I + k_3))exp(\frac{h}{2}\hat{D})[A_I + k_3] \\
A(z+h,T) &= exp(\frac{h}{2}\hat{D})[A_I + k_1/6 + k_2/3 + k_3/3] + k_4/6
\end{aligned} \tag{2.16}$$

2.2 Pulse Propagation in Multimode Fibers

Multimode fibers are generally considered as complex and chaotic thus mainly used for beam delivery applications and imaging purposes. Categorization of multimode fibers can be done according to their core number and index of refraction. As it shown in Fig. 2.2, single-core multimode fibers can be classified as step-index and graded-index multimode fibers according to their index profiles. This index profile difference leads to significant changes in pulse propagation. Grade-index profile leads to equal spacing of the modal wave numbers for GIMFs thus creates natural periodic self-imaging for the propagating beam inside the fiber. Since the periodic self-imaging allows strong nonlinear coupling among the modes, GIMFs offers undiscovered spatiotemporal nonlinear dynamics to study.

2.2.1 Spatiotemporal Nonlinear Phenomena in Graded-index Multimode Fibers

GRIN fibers are suitable test beds for spatiotemporal nonlinear optical studies due to their relatively low modal dispersion and periodic self-imaging pattern for

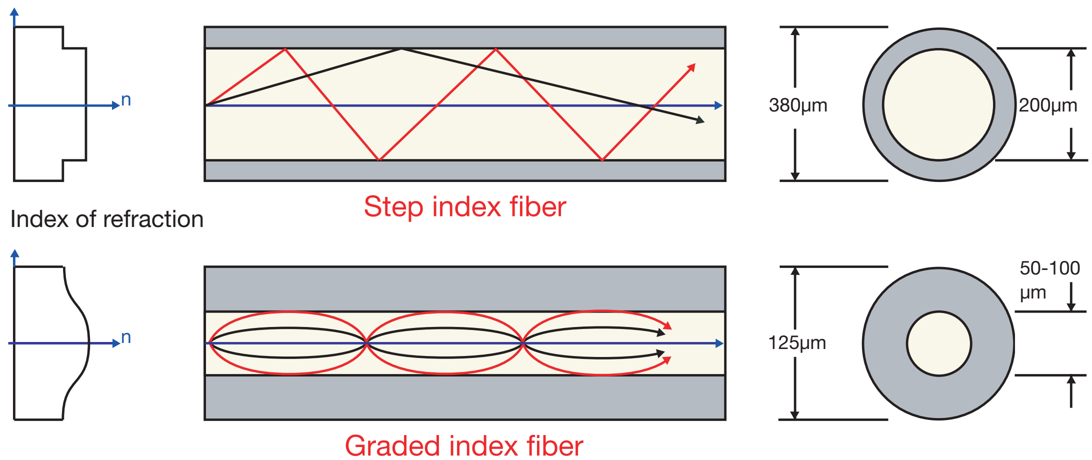

Figure 2.6: Types of single-core multimode optical fibers. Refractive index profiles are indicated on the left column.

propagating beam. This unique propagation behavior enables nonlinear coupling between the fiber modes and triggers various nonlinear phenomena.

In the recent years because of the aforementioned reasons GRIN fibers attracted huge attention from the nonlinear fiber optics community. In 2013, Pourbeyram et al. discovered cascaded Raman scattering using a GRIN fiber with 50 μm core diameter and observed 20 cascaded peaks which cover a span from 523 nm to 1750 nm [12]. Later, Renninger et al. reported formation of multimode solitons by pumping GRIN fiber with 300 fs pulses at 1550 nm in 2013 [13].

In 2015, Wright et al. studied generation of dissipative waves using pump pulses at anomalous dispersion as well [17]. They numerically confirmed that the observed wavelength conversion is heavily depending on spatiotemporal oscillations inside the GRIN fiber. Even though theoretical predictions published in 2003, Krupa et al. reported first experimental demonstration of geometric parametric instability in 2016 [16]. By using a 900 ps pump pulses at normal dispersion to excite GRIN fiber with 50 μm core diameter they obserbed sidebands with 120 THz frequency shift. Krupa et al. also reported self-beam cleaning in 2016 as well [14]. With these remarkable phenomenon while the beam propagates and experiences periodic self-imaging inside the GRIN fiber non-Gaussian beam evolves to Gaussian profile in space. Experimental studies presented that one can increase the quality of a beam with $M^2 = 7$ to $M^2 = 2$. Later Liu et al. reported this phenomenon for ultrashort pulses [29].

On the other hand, Lopez-Galmiche et al. reported the first supercontinuum generation in GRIN fibers with using 400 ps pump pulses with 185 kW peak power [15]. The reported supercontinuum evolution benefits combination of different nonlinear processes such as geometric parametric instability, SRS, four-wave mixing and harmonic generations with relatively long test fiber (28.5 m).

In 2017, Teğin et al. demonstrated geometric parametric instability (spatiotemporal instability) with femtosecond pump pulses first time in the literature [18]. This study verified the recently proposed spatiotemporal nonlinear attractor model which can explain the self-beam cleaning and spatiotemporal instability effects at the same time [30]. Later Teğin et al. reported first octave spanning supercontinuum generation based on cascaded-Raman scattering in GRIN fibers and obtained 4 W output average power with 2 MHz pump pulses [19]. In this theses femtosecond spatiotemporal instability and cascaded-Raman scattering based watt-level supercontinuum studies are explained in details at Chapter 3 and Chapter 4, respectively.

2.2.2 Numerical Modeling of Multimode Pulse Propagation in Optical Fibers

Since spatial evolution along the propagation is also plays a significant role for multimode fibers, numerical calculations become time consuming and complex. Different numerical approaches are presented in the literature to overcome these issues and to study spatiotemporal nonlinearities in multimode fibers. The main difference between these methods are computational complexity with certain simplifications.

The most general numerical method to simulate pulse propagation in multimode fibers is (3+1)D NLSE which also called as Gross-Pitaevskii equation (Eq. 2.17). This nonlinear wave equation considers evolution of the total field in four dimensions thus numerical calculations complexity is high due to the requirements of multidimensional Fourier transformations. To reduce computational times simplifications such as y=0 could be applied to (3+1)D NLSE [31]. In the literature, to introduce graded-index profile $n(x, y)^2 = n_{co}^2(1 - 2\Delta r^2/R^2)$ should be considered in numerical calculations for $r < R$ and $n(x, y) = n_{cl}$. Where n_{co} is the maximum of the core refractive index, n_{cl} is the refractive index of clad and Δ is the relative index difference defined as $\Delta = (n_{co}^2 - n_{cl}^2)/2n_{co}^2$.

$$\frac{\partial A}{\partial z} = i\frac{1}{2k_0}\left(\frac{\partial^2 A}{\partial x^2} + \frac{\partial^2 A}{\partial y^2}\right) - i\frac{\beta_2}{2}\frac{\partial^2 A}{\partial T^2} + i\gamma\,|A|^2\,A - i\frac{k_0\Delta}{R^2}(x^2 + y^2)A \tag{2.17}$$

The (3+1)D NLSE can be solved numerically with SSFM or RK4IP techniques but simulating 50 m GIMF requires more than 15 days even with a modern simulation computer [13]. To overcome this issue the common method is decreasing the pump pulse duration and fiber length at the same time but such simplifications can be misleading since order of magnitude changes in pulse duration or peak power may trigger different nonlinearities [16].

Later Poletti et al. [32] introduced coupled-mode technique to simulate multimode fibers with more fast and accurate way. For each mode an evolving envelope A_p is considered and the sum of these envelopes according to the function of the modes compose the the complex electric field (Eq. 2.18).

$$E(\rho, \phi, \omega) = \sum_p F_p(\rho, \phi, \omega)e^{i\beta_p(\omega)z}A_p(z, \omega) \tag{2.18}$$

Here, decomposition of the field should be calculated for the specific test fiber and parameters should be defined for the test fibers index-profile. The nonlinear coupling term is for each evolving envelope a propagation equation similar to NLSE or GNLSE can be considered as it follows.

$$\frac{\partial A_p}{\partial z} = i\delta\beta_0^{(p)} A_p - \delta\beta_1^{(p)} \frac{\partial A_p}{\partial t} - i\frac{\beta_2^{(p)}}{2}\frac{\partial^2 A_p}{\partial^2 t} + i\frac{\gamma}{3}(1 + \frac{i}{\omega_0}\frac{\partial}{\partial t})\sum_{l,m,n}\eta_{plmn}$$
$$\times[(1 - f_R)A_l A_m A_n^* + f_R A_l \int h_R A_m(z, t - \tau)A_n^*(z, t - \tau)d\tau] \tag{2.19}$$

In this model while the field propagates inside the multimode fiber interaction between the modes are introduced via nonlinear coupling parameter η_{plmn}. With the coupled-mode technique one needs to choose the considered number of modes in calculations. In general multimode fibers can support hundreds of modes but according to the considered test fiber simplifications can be made. As an example Mafi modified the coupled-mode technique for GIMFs by considering linearly polarized and radially symmetric modes [33]. With these assumptions one can calculate nonlinear coupling among the modes of GIMF as shown in Eq. 2.20 where L_p, L_l, L_m and L_n are Laguerre polynomials.

$$\eta_{plmn} = 2\int_0^\infty e^{-2u} du L_p(u)L_l(u)L_m(u)L_n(u) \tag{2.20}$$

Very recently a fast pulse propagation model is introduced for GIMFs. Here researchers considered natural self-imaging effect of the GIMF and periodically oscillate the nonlinearity parameter $\gamma(z)$ along the propagation direction in NLSE and GNLSE [34, 35]. This method allows the simulations of long fiber lengths with manageable computation times but spatial evolution of the propagating beam cannot be investigated with this method.

$$\frac{\partial A}{\partial z} + \left(\sum_{n\geq 2}\beta_n \frac{i^{n-1}}{n!}\frac{\partial^n}{\partial t^n}\right) A = i\gamma(z)\left(1 + \frac{\partial}{\partial t}\right)$$
$$\times\left((1 - f_R)A\left|A\right|^2 + f_R A\int_0^\infty h_R(t')\left|A(z, t - t')\right|^2\right) \tag{2.21}$$

In this method the periodic modulation is introduced to nonlinearity term as $\gamma(z) = \omega_0 n_2/(cA_{eff}(z))$ where ω_0 is central frequency, c is speed of the light and $A_{eff}(z)$ is the effective beam area of the propagating pulse. The effective beam area of the propagating pulse which experiences periodic self-imaging can be approximated as

$$A_{eff}(z) = 2\pi a_0^2[cos^2(\sqrt{g}z) + \frac{1}{\beta_0^2 a_0^4 g} sin^2(\sqrt{g}z)] \tag{2.22}$$

$g = 2\Delta/r_c^2$ where r_c is fiber core radius, $\Delta = (n_{core}^2 - n_{clad}^2)/2n_{core}^2$ is the relative index difference between the core and the clad of the fiber and $\beta_0 = \omega_0 n_0/c$ where n_0 is the core refractive index (at the center of the fiber). An example Python code based on this algorithm is presented in Appendix A of this thesis.

2.3 Pulse Generation in Fiber Lasers

Optical fibers can be doped with rare-earth elements to use as a gain segment inside a optical cavity. By implementing various techniques to the cavity mode-locking can be performed to achieve ultrashort pulses. Starting with neodymium-doped optical fibers mode-locked fiber lasers studied over the last three decades [5]. Since 1991, researchers show great attention to the erbium-doped fibers based oscillators to investigate soliton dynamics [36]. Various output parameters of a mode-locked fiber laser are subjected to studies to increase the capability of fiber based laser technologies such as average power, pulse duration and energy.

Since soliton pulses are limited in terms of pulse energy different pulse types are discovered with investigating pulse dynamics extensively inside the laser cavity. First approach of the community to this problem was dispersion mapping. Since Er, Tm and Ho wavelengths are at negative dispersion regime one can introduce positive dispersion to the cavity with gratings and special fibers. With this technique all-fiber Er based mode-lock oscillator with sub-100 fs pulse duration is demonstrated [37].

Later Ytterbium based fiber lasers are generally preferred in the mode-lock fiber lasers due to its high and broadband gain. The similar methods which studied with Erbium-doped fiber lasers are also introduced to Ytterbium-based cavities and 1.5 nJ sub-40 fs pulses demonstrated with dispersion-managed cavity design [38]. First in the amplification stage later with a mode-locked cavity design researchers discovered parabolic pulses benefiting dispersion mapping tehcnique [7, 8]. However, a certain degree of dispersion mapping inside the laser cavity is necessary to achieve stable mode-locking operation in a fiber laser cavity due to thermal drift and degradation of the optical alignments. Additionally, at 1μm wavelength range negative dispersion can be implemented by bulk grating or photonic crystal fibers which results in increased complexity and undermines benefits of fiber lasers such as compactness and stability. Later, a stable passively mode-locked all-normal dispersion fiber laser is demonstrated and pulse generation is attributed to the strong spectral filtering of chirped pulses [9]. Over the last decade, all-normal dispersion fiber lasers are studied extensively by exploiting dissipative soliton pulse dynamics [39]. In the literature, the power and energy scalability of the dissipative soliton pulses are demonstrated with very-large-mode-area fibers [40, 11].

In addition to cavity dynamics different mode-locking methods are proposed for fiber laser systems as well. Among them nonlinear polarization evolution (NPE) method become commonly used for mode-lock fiber lasers. Besides the NPE, nonlinear optical loop mirror and nonlinear amplifying loop mirror methods also introduced in the literature [41, 42]. In the literature sub-200 fs all-fiber and environmentally stable cavity designs with nonlinear loop mirror methods are presented [43]. On the other hand material-based saturable absorbers introduced with the development of 2D materials and nanotechnology [44, 45]. Most commonly used and commercially available saturable absorber is semiconductor saturable absorber mirror (SESAM). SESAM can be implemented in an enviromentally stable linear cavity mode-lock fiber laser design to obtain femtosecond pulses [46].

Chapter 3

Spatiotemporal Instability of Femtosecond Pulses

3.1 Introduction

Among the recently discovered spatiotemporal nonlinear effects in GIMF, spatiotemporal instability, called also as geometric parametric instability (GPI) in the literature, is an outstanding wavelength conversion technique. Due to generated instability sidebands have remarkable frequency shift and inherit the spatial beam shape of the pump pulses this new method can be implemented to various applications which requires specific wavelengths from a fiber source [16, 30].

In 2003, theoretical work presented by Longhi and predicted geometric parametric instability effect in multimode fibers [47]. The necessary quasi-phase matching condition between the pump, signal and idler is provided by the natural periodic refocusing of the propagating beam inside the GIMF. When the conditions are satisfied this unique propagation results as spatiotemporal instability sidebands and discrete peaks appear in the spectrum with large frequency shift. Here one should notice that the intermodal four-wave mixing is also capable to generate spectral peaks with the same amount of frequency shifts but spatiotemporal instability peaks inherit the spatial mode profile of the pump source [48].

In the literature, Krupa et al. reported the first experimental observation of spatiotemporal instability sidebands by using quasi-continuous pulses and reported sidebands are detuned more than 100 THz from the pump frequency [16]. Very recently, Wright et al. [30] studied the internal dynamics of the self-beam cleaning and spatiotemporal instability generation in GIMFs and presented a theoretical model to explain the connection between these spatiotemporal effects by introduced an universal attractor model. The preliminary connection between these nonlinear phenomena is experimentally noticed by Lopez-Galmiche et al. in their supercontinuum generation study with GIMF [15].

So far the studies about on spatiotemporal instability focused on quasi-continuous pulse evolution in graded-index MMF at the normal dispersion regime. We believe this tendency is due to the analogy between GPI and well-known modulation instability in single mode fibers presented by Longhi's theoretical work [47]. Eventhough spatiotemporal instability has a great potential as a new wavelength conversion method because of these reasons spatiotemporal dynamics of femtosecond pulses are generally neglected. So far in the literature only self-beam cleaning effect is studied with femtosecond pulses [29].

In this chapter, we investigated the evolution of femtosecond pulses in a GIMF segment and observed the spatiotemporal instability of ultrashort pulses in GIMF for the first time in the literature. In experiments, as a pump source, we used a commercial Ti:Sapphire laser system which is capable to generate linearly polarized 200 fs pulses at 800 nm. We studied the evolution of these pulse inside 2.6 m GIMF with 50 μm core diameter both experimentally and numerically. Observed Stokes sidebands appeared in the spectrum with 91 THz frequecny shift. Spatial beam shape of first instability Stokes is measured and features Gaussian-like near-field beam profile. This measurement verifies that our observation is spatiotemporal instability rather than intermodal four-wave mixing. Numerical simulations confirm the experimental observations on the spatiotemporal instability. Calculations also provide information on the spatial evolution of pump field and sidebands inside as well. Our results contradicts with Longhi's model which is not applicable to ultrashort pump pulses. But with the self-beam cleaning of ultrashort pulses presented by Liu et al. [29], our results validate the universal attractor model presented by Wright et al [30].

3.2 Numerical Study

Numerical simulations are performed to investigate ultrashort pulse propagation in GIMF with using using the generalize multimode nonlinear Schödinger equation [32, 49, 33]. The detailed explanation of this model presented in Chapter 2 of this thesis. To solve Eq.(2.19) numerically, we use symmetrized split-step Fourier method [1] and include Raman process and shock terms in our simulations. We consider n_0 as 1.4676, n_2 as $2.7x10^{-20}m^2/W$, relative index difference as 0.01, integration step as 10 μm, time window width as 15 ps with 2 fs resolution in our simulations.

In the numerical studies we investigated the ultrashort pulse propagation in a GIMF with 50 μm core diameter as a test fiber. Such a fiber supports 415 modes at 800 nm but simulating all of them will require time-consuming calculations. To achieve manageable computation times, we only consider first six zero-angular-momentum modes in our simulation. In the numerical studies pump pulse parameters are defined as 200 fs pulse duration, 350 nJ pulse energy and 800 nm central wavelengths. The initial pulse energy is splited among the six mode as 50% in p=0, 18% in p=1, 13% in p=2, 10% in p=3, 6% in p=4 and 3% in p=5.

Femtosecond pulse propagation is studied for 30 cm GIMF. Spectral and temporal evolution is presented in Fig. 3.1. In frequency domain, pump pulse experiences broadening while propagating inside the GIMF. This behavior is unique feature of GIMF and a result of high pump pulse energy [50, 51]. For the applied simulation parameters, after exposing to periodic self-imaging effect approximately 100 times sideband formation is observed in numerical studies. First pair

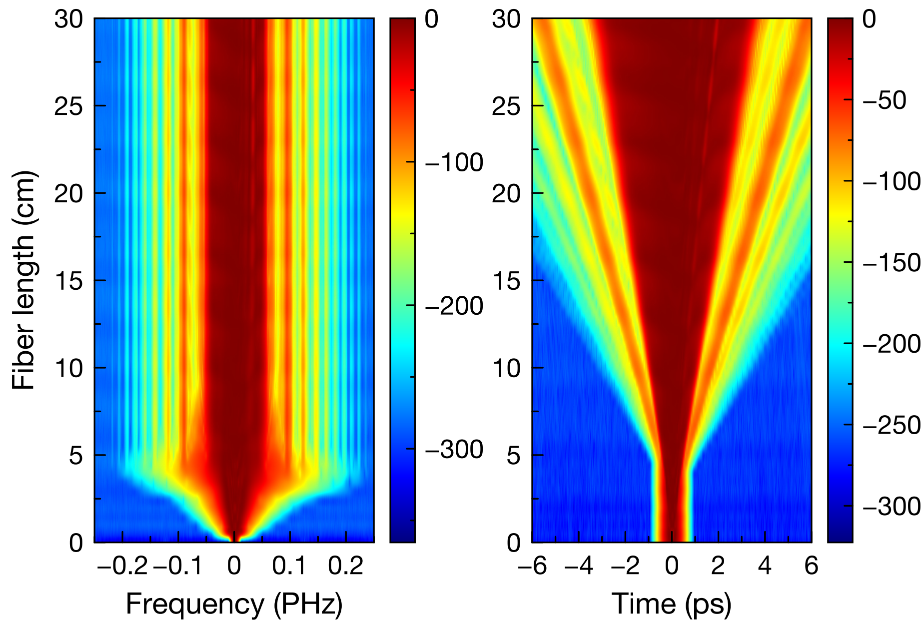

Figure 3.1: Results from the numerical simulation showing total evolution through 30 cm fiber in frequency and time domains. The intensities in dB scale.

of sidebands are detuned approximately 90 THz from the launched pump pulse frequency in frequency domain. This frequency shift corresponds to 1055 nm for Stokes sideband and 640 nm for anti-Stokes sideband. After emerging sidebands started to grove as a result of continuing frequency conversion while propagation. At the end of the considered fiber length (30 cm) intensity difference between sidebands and the pump are observed is 65 dB.

Since it has a great importance we presented spatial changes in propagation as well (Fig. 3.2). Our results also indicates that the propagating beam experiences periodic refocusing along the GIMF. For different points spatial profiles are presented during the propagation in Fig. 3.2(a).a, Fig. 3.2(a).c and Fig. 3.2(a).e. After propagating ($\sim$ 5 cm) sideband generation occures and we noticed a non-Gaussian intensity distribution for total field Fig. 3.2(a).b. From simulation results we extract spatial intensity distribution of first instability Stokes as well. Our results indicate that Stokes sideband inherits its the spatial distribution from the pump pulse and preserves while the propagation (Fig. 3.2(a).c-f). This observation is a signature of the spatiotemporal evolution of the instability.

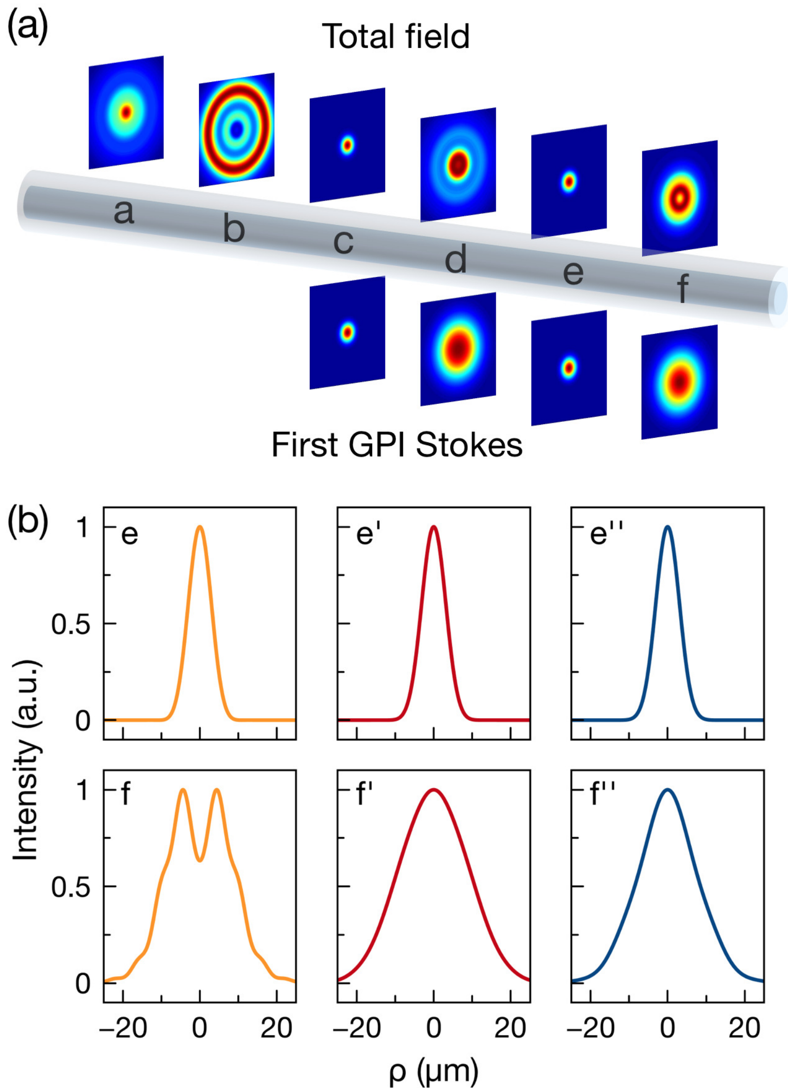

Figure 3.2: Numerical results for spatial evolution inside the graded-index MMF with 50μm core diameter. (a) Spatial intensity distributions at 2 cm, 5 cm, 17.03 cm, 17.12 cm, 17.21 cm, 17.28 cm (a-f). (b) Beam profiles of total field (e, f), first Stokes sideband (e', f') and first anti-Stokes sideband (e", f") for 17.21 and 17.28 cm of the fiber, respectively.

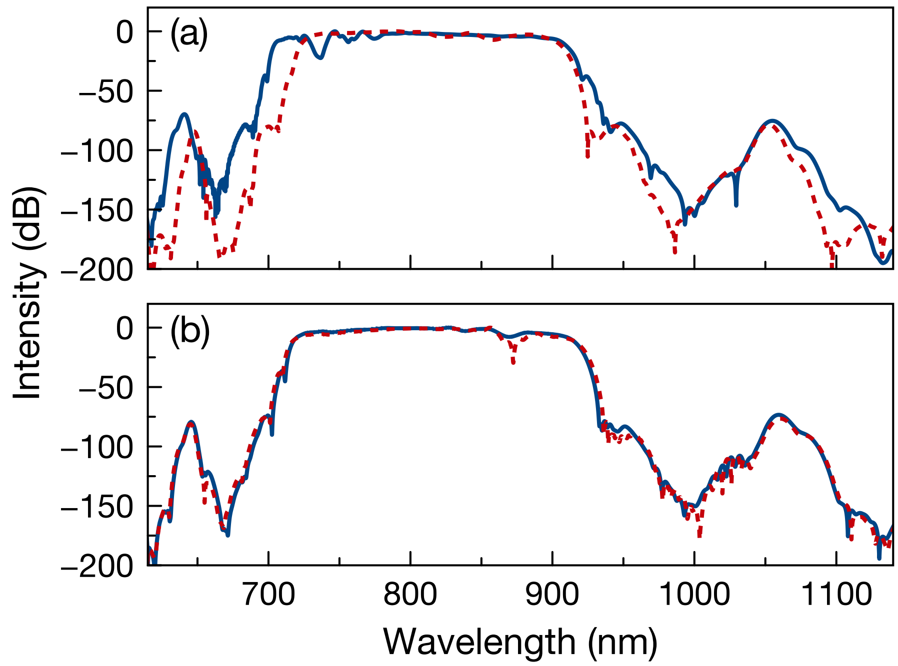

Figure 3.3: Numerical spectra obtained from 30 cm graded-index MMF with different parameters. (a) Calculations with 6 cylindrically symmetric modes for different initial energy distributions (b) calculations with 3 cylindrically symmetric modes for different initial energy distributions.

Later we consider the effect of different launch conditions on our numerical calculations. We compared above mentioned result (solid line) with the following case 28.6% in p=0, 23.8% in p=1, 19.04% in p=2, 14.28% in p=3, 9.52% in p=4 and 4.76% in p=5 (dashed line) and presented in the Fig.3.3(a). The decrease in the fundamental mode caused less spectral broadening and indirectly creates a slight frequency shift to first anti-Stokes sideband. We observed 4 dB intensity difference between the considered energy distribution cases. Next, we studied the effect of considered number of modes in numerical calculations. To create a significant change we only consider first three zero-angular-momentum modes with different initial energy distributions. For the same propagation length (30 cm) calculated results are presented in the Fig.3.3(b). We considered two different excitation condition for our simulations with three modes as 50% in p=0, 30% in p=1, 20% in p=2 (solid line) and 35% in p=0, 35% in p=1, 30% in p=2 (dashed line). We noticed simulations converges to similar formation except the intensity of generated sidebands. Our calculations suggests that increasing considered number of fiber modes ensures higher conversion efficiency.

3.3 Experimental Results and Discussions

We performed experiments by an amplified Ti:Sapphire laser (Spitfire by Spectra-Physics). The pump source is capable to generate linearly polarized, single-mode, 200 femtosecond ultrashort pulses at 800 nm with 1 kHz repetition rate. Encouraged by the simulations we chose a commercially available GIMF (Thorlabs-GIF50C) with 50 μm (125 μm) core (clad) diameter and 0.2 numerical aperture as our test fiber. To excite the 2.6 m test fiber we employed a plano-convex lens and three-axis translation stage. We selected 60 mm focal length lens to create ~ 20 μm waist size on the test fiber facet. This also ensured free space coupling efficiency greater than 80%.

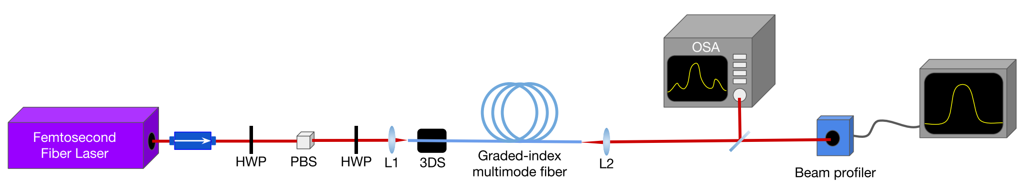

Figure 3.4: Schematic of the experimental setup comprising of half-wave plate (HWP), three-dimensional stage (3DS), polarizing beam splitter (PBS), optical spectrum analyzer (OSA).

Experimentally obtained results are presented in Fig. 3.5 for different launched pulse energy. As simulations suggested pump pulse experiences asymmetric spectral broadening. We believe the assymmetric broadeding in frequency domain could be the result of stimulated Raman scattering (SRS). For 345 nJ launch pulse energy we noticed further spectral broadening but SRS peak formation is not achieved. On the contrast, at 295 nJ we obtained first instability Stokes sideband. Theory and simulation indicate that Stokes and anti-Stokes sidebands should appear at the same time for spatiotemporal instability. Thus the anti-Stokes sideband is under the noise level of the optical spectrum analyzer. At 320 nJ pump pulse energy we obtained anti-Stokes sideband as well. With increasing the launch pump pulse energy amplification and broadening of the Stokes and anti-Stokes sidebands are recorded.

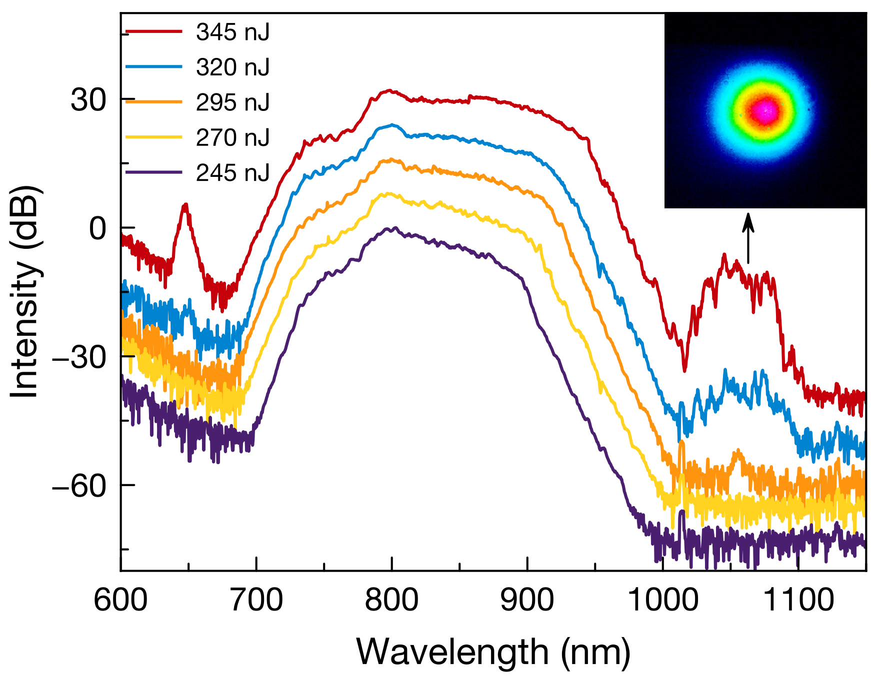

Figure 3.5: Measured spectra as a function of launched pulse energy. Inset: near-filed beam profile of first Stokes sideband.

Experimentally obtained results are well matched with numerical calculations. Spatiotemporal instability peak pair is observed with $\sim$ 91 THz frequency shift from the pump pulse frequency (Fig. 3.5). This shift corresponds to 1055 nm and 645 nm for first Stokes and anti-Stokes respectively. In wavelength domain spectrum bandwidth of first Stokes and anti-Stokes are $\sim$ 12 nm and $\sim$ 5 nm, respectively but in frequency domain sidebands have similar bandwidths as 3.2 THz. We experimentally obtained the near-field beam profile of the first Stokes sideband with longpass filter (see Fig.3.5-inset). As expected from a spatiotemporal instability sideband, a clean (speckle free), Gaussian-like near-field beam profile is observed which is similar to the pump beam shape.

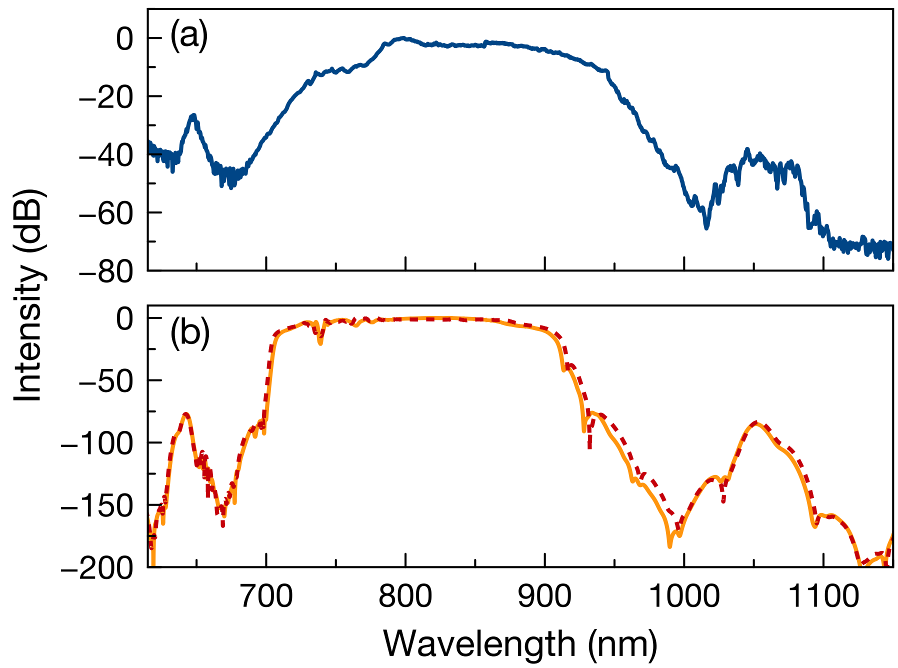

Figure 3.6: Optical spectra obtained after propagating 2.6 m graded-index MMF. (a) Experimental measurement and (b) simulation results for different energy distribution between the modes.

To investigate the difference of experimental studies with the numerical calculations, we simulate 2.6 m GIMF with similar parameters used in our experiments (Fig. 3.6). Here we considered first three zero-angular-momentum modes with included Raman process and shock terms. First, we distributed 345 nJ pulse energy of the launched pulse to modes such as 50% in p=0, 30% in p=1 and 20% in p=2 (solid-line). Later we changed the splitting ratio between the modes as 35% in p=0, 35% in p=1 and 30% in p=2 (dashed-line). For both distributions, positions and bandwidths of instability sidebands in frequency domain are similar to experimentally obtained results. We believe with increasing considered number of fiber modes more realistic results can be obtained from numerical simulations.

3.4 Conclusion

To conclude, in this chapter we presented the spatiotemporal instability of ultrashort pulses in GIMF. We obtained spatiotemporal instability formation with femtosecond pump pulses first time in the literature. Our experimentally results are verified with numerical studies as well and presents good match. Detailed numerical studies revealed the generation and propagation behaviors of instability sidebands inside of MMF. Our results also verifies the recently presented universal attractor model for the nonlinear pulse propagation in GIMFs [30]. We strongly believe with the intrinsic large frequency shift, spatiotemporal instability sidebands can be employed to generate ultrashort pulses with desired wavelengths for various application purposes.

Chapter 4

Cascaded Raman Scattering Based Supercontinuum Generation

4.1 Introduction

In single mode or few-mode optical fibers supercontinuum generation is studied extensively in the literature [52, 27]. With the developments in photonic crystal fiber technology, supercontinuum sources reached broad wavelength ranges and octave-spanning become accessible. Nowadays, supercontinuum sources based on fiber technologies are generally preferred in optical metrology, fiber communication systems and biomedical imaging [53]. Very recently, GIMF based supercontinuum generation studies are presented by simultaneously exploiting spatiotemporal nonlinear effect in normal dispersion regime in the literature[15, 54].

First normal dispersion supercontinuum generation in GIMF is reported by Lopez-Galmiche et al. by employing an enormous pump peak power (185 kW) [15]. Lopez-Galmiche et al. achieved supercontinuum formation from supercontinuum from spatiotemporal instability, SRS and harmonic generation in 28.5 m graded-index MMF with 400 ps pulses at 1064 nm. Later Krupa et al. presented the interplay between spatio-temporal instability and SRS while spatiotemporal instability peaks evolves to a supercontinuum [54]. By intentionally selecting high peak power and low repetition rate sources, these studies benefited from the combination of different nonlinearities to achieve supercontinuum. They reached ∼50 mW output average power with 500 Hz and ∼700 mW with 30 kHz, respectively. Thus maximum average power of the reported octave-spanning supercontinua is in milliwatts range so far even though graded-index MMF is promoted with high power level handling potential.

In this chapter we demonstrated a cascaded Raman scattering-based novel approach to generate octave-spanning watt-level and high repetition rate supercontinua in graded-index MMFs. We developed an all-fiber laser system capable to generate 70 ps pulse duration at 1040 nm with MHz repetition rates, ∼30 kW peak power as a pump source to investigate supercontinuum dynamics. Inside the GIMF the pump pulses are evolved to a spectrally flat octave-spanning supercontinua with multi-watt average output powers. We numerically and experimentally investigated the formation and spectral evolution of the supercontinuum. The effect of propagation length and GIMF core size is reported experimentally as well. The potential of GIMF is presented by scaling pump pulse repetition rate from 200 kHz to 2 MHz while peak power of the pump pulses remains same. With this method the average supercontinuum output power is increased from 350 mW to ∼ 4 W while supercontinuum spectra preserved. Experimental studies revealed that spatial distribution of the obtained supercontinua in graded-index MMF features Gaussian-like beam shape.

4.2 Experimental Results

We developed a home-built all-fiber laser as a source to perform supercontinuum experiments in GIMF. Fig. 4.1 presents the schematic of the experimental setup. Yb-doped dispersion managed mode-locked fiber laser with 44 MHz repetition rate is employed as a pump pulse generator [55]. The oscillator generates 2 ps positively chirped pulses at 1035 nm. Output pulses of the fiber oscillator are characterized in spectral, temporal and frequency domains (see Fig. 4.2 and Fig. 4.3).

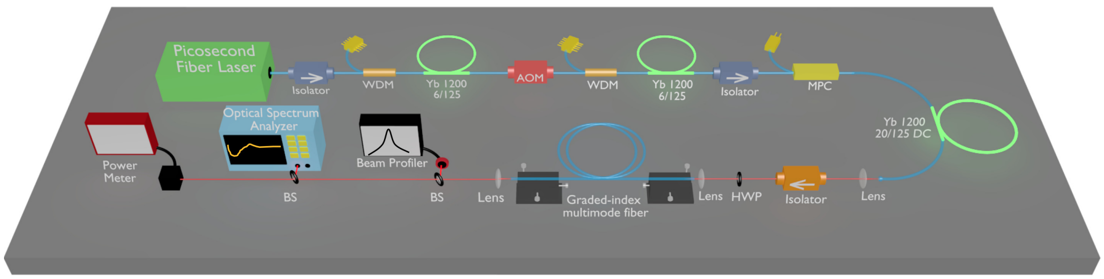

Figure 4.1: Schematic of the experimental setup comprising of Yb-doped fiber, wavelength division multiplier (WDM), beam splitter (BS), acousto-optic modulator (AOM), multi-pump combiner (MPC), three-dimensional stage (3DS), half-wave plate (HWP).

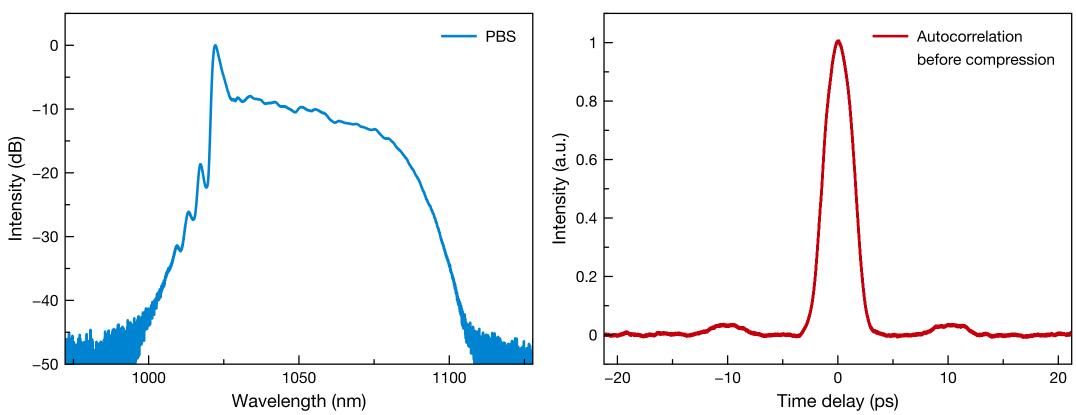

Figure 4.2: Spectral and temporal measurement results obtained from NPE output port (PBS) of the fiber oscillator.

To avoid nonlinear effect in amplification stages, generated pulses are chirped by a fiber stretcher. After the first preamplifier segment these chirped pulses are amplified to ∼70 mW average power. Acusto-optic modulator (AOM) is preferred to manipulate the repetition rate of the pulse train before the boost amplifier to achieve sufficient peak power for supercontinuum studies. Because of the intrinsic losses of AOM and the manipulation of the repetition rate from 45 MHz to 200 kHz - 2 MHz range, average power drops to <5 mW after the AOM. An additional preamplifier is employed before the double clad boost amplifier to eliminate generation of amplified stimulated emission. At the end of Yb-doped double clad boost amplifier segment, we achieved 70 ps pulses with ∼30 kW peak power centered around 1045 nm with ∼20 nm bandwidth and adjustable repetition rate.

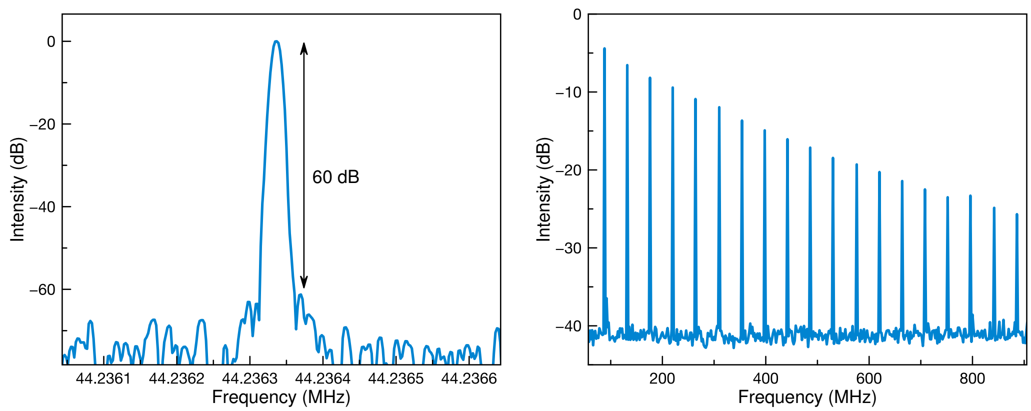

Figure 4.3: Characterization of the mode-lock oscillator in RF domain.

With a biconvex lens we collimated the amplified pump pulses and employed a high power free-space isolator to eliminate the back reflections. We employed a half-wave plate to change the polarization axis of the linearly polarized pump pulse since Raman gain is polarization dependent [1]. To create ~ 20 μm beam waist size at the fiber facet we prefered a biconvex lens with 2 cm focal length. The free space coupling efficiency greater than 80% is ensured with a three-axis translation stage.

Firstly we selected a 20 m GIMF with 62.5 μm core diameter as a test fiber and investigate the supercontinuum generation in details as a function of pump power (Fig. 4.4). When we reached to 510 mW output average power, eneration of cascaded SRS with ~ 13 THz frequency shifts is observed as demonstrated by Pourbeyram et al. [12]. Generation of intense SRS peaks up to fifth Stokes is presented in details (see Fig. 4.4(b,c)). This uniquely strong Raman scattering effect can be explained with multimode propagation in side the GIMF. As presented for intermodal four-wave mixing [56], generated Raman Stokes propagates in the higher order modes as well [12]. This special propagation pattern can balance the velocity mismatch between the pump pulse and Raman Stokes and triggers the generation of cascaded Raman scattering in GIMF. We observed that when SRS peaks reach zero dispersion wavelength (ZDW) of the fiber (∼ 1330 nm), Raman Stoke generation stops because of the reduction of Raman gain in the vicinity of the ZDW [57]. Above the ZDW, instead of Raman Stokes a broad spectral formation emerges at 1500 nm. In the literature this formation is explained as complex parametric phenomena including collision based spectral broadening [27, 58].

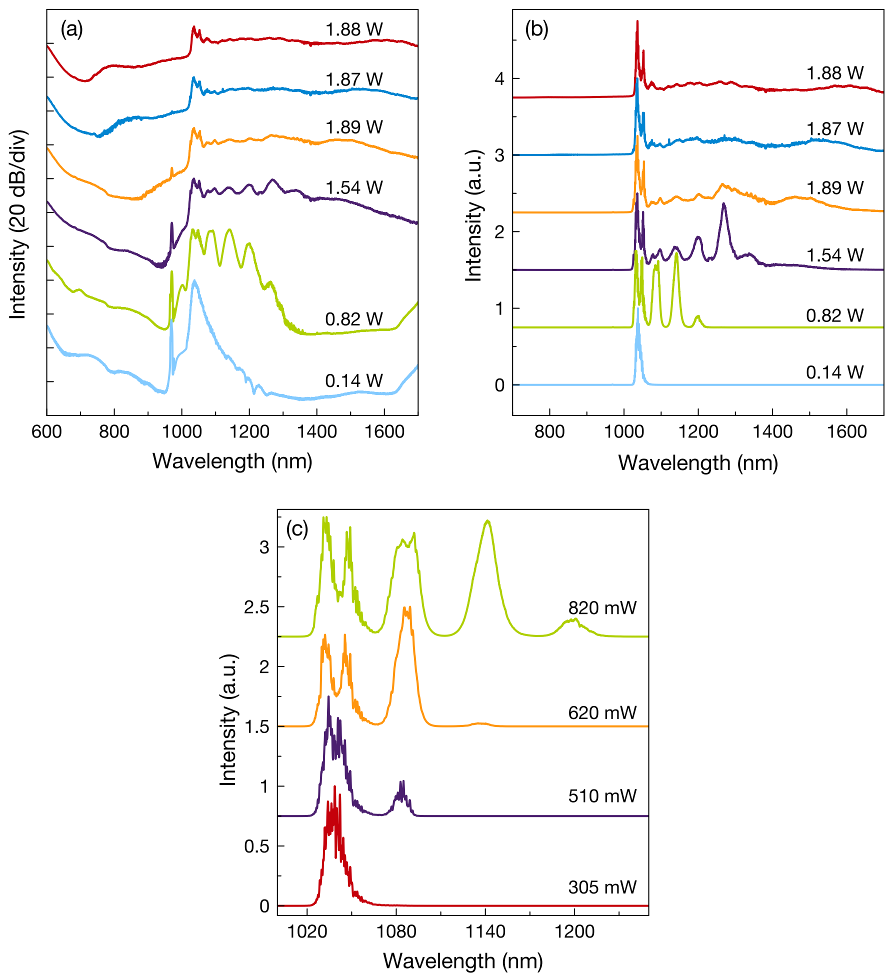

Figure 4.4: Variation of 20 m graded-index MMF as a function of launched pulse average power recorded for 1 MHz pump pulse repetition rate presented in (a) logarithmic and (b) linear scale. (c) Formation of cascaded SRS peaks. Output average powers indicated for each spectrum.

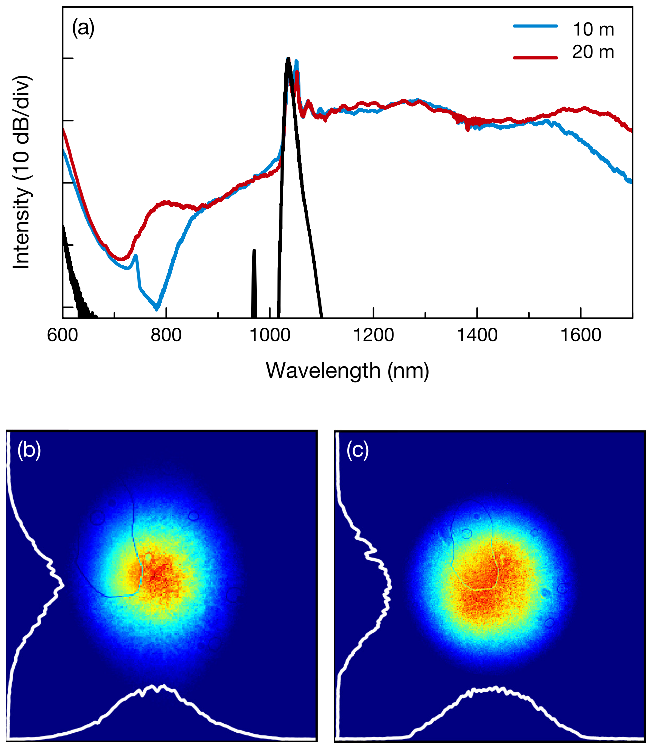

Figure 4.5: (a) 10 m and 20 m graded-index MMF for 1 MHz pump pulse repetition rate. Spectrum of pump pulse is presented as black. Near-field beam profile for (b) 730 nm to 1200 nm range and (c) 1100 nm to 1200 nm range of the supercontinuum.

After 1.89 W output average power is achieved, we observed the generation of shorter wavelength of the supercontinuum formation. Since the operation bandwidth of GIMF is defined as 800 nm to 1600 nm we recorded small decrease at average power during this formation. The formations at the visible spectrum can be explained with generation of anti-Stokes wavelength even without proper phase-matching as explained for the supercontinuum generation for picosecond pulses in photonic crystal fibers [59, 60]. At the end spectrally flat octave-spanning supercontinuum is generated with 1.88 W average output power for 1 MHz pump repetition rate. Calculated spectral intensity deviation of the continuum is 52%. For the wavelengths higher than the pump wavelength (between 1060-1700 nm), spectral intensity deviation calculated to 24%. We strongly believe that the cascaded SRS peaks provides this remarkable spectral flatness.

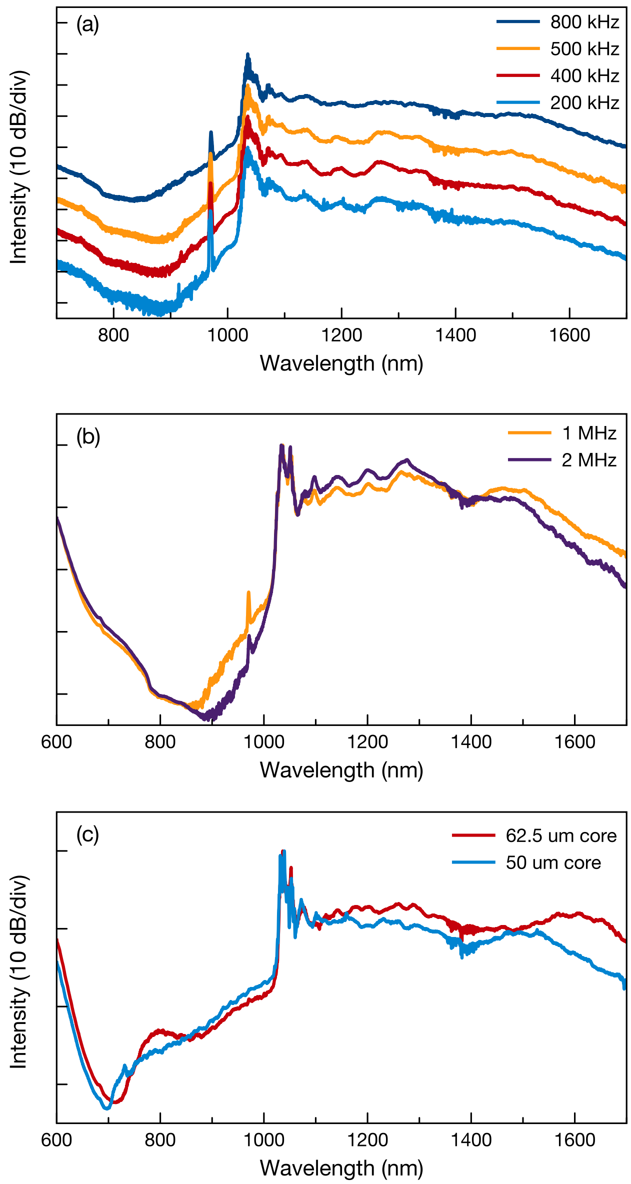

Figure 4.6: (a) Supercontinuum spectra measured from 20 m graded-index MMF (62.5 μm core diameter) 200 kHz to 800 kHz repetition rates for constant peak power. (b) Supercontinuum spectra measured from 20 m graded-index MMF (62.5 μm core diameter) for MHz repetition rates with same peak power. (c) Obtained supercontinuum spectra with 1 MHz pump pulses for graded-index MMFs with different core diameters.

To study the effect of propagation length on supercontinuum generation, we changed the test fiber length from 20 m to 10 m and performed the experiments for the same conditions again. We noticed that average power increased from 1.88 W to 2.19 W. This difference shows that some portions of the supercontinuum experiences fiber loss while propagation but spectral width and flatness of generated supercontinuum is decreased for 10 m test fiber length (Fig. 4.5(a)). When we compare the results of Pourbeyram et al. [12] with our observations, we strongly believe that since our pump pulse wavelength is relatively close to ZDW of the GIMF fiber we achieved the supercontinuum generation. Our results presents strong soliton generation above the ZDW of the test fiber is crucial to obtain supercontinuum formation in GIMFs.

To encourage possible applications we measured the spatial properties of the generated supercontinuum. We performed near field spatial distribution measurements with a beam profiler. Since the measurement tool can operate up to 1200 nm, spectral distribution of the supercontinuum beam from 730 nm to 1200 nm is presented in Fig. 4.5(b). We introduced a longpass-filter to select the spectral content between 1100 nm and 1200 nm and present in Fig. 4.5(c). Surprisingly, Gaussian-like spatial profile with high-order modes in the background is observed for both measurements even though GIMF can support hundreds of modes. Similar spatial distributions are reported by previous studies on supercontinuum generation in GRIN multimode fibers [15, 54]. Our results suggest Raman and Kerr beam cleaning could be the reason of measured Gaussian-like beam profiles Similar spatial distributions are reported by previous studies on supercontinuum generation in GRIN multimode fibers [15, 54].

To demonstrate the versatilely of our novel supercontinuum generation method we scaled the pump pulse repetition rate from 200 kHz to 2 MHz while the peak power remains same. This method allowed us to scale the output power while the supercontinuum preserves its features. First we concerned the kHz range for fixed pump peak power (25 kW) for 20 m test GIMF Fig. 4.6(a). The measured average output powers are 350 mW, 700 mW, 875 mW and 1.4 W for 200 kHz, 400 kHz, 500 kHz and 800 kHz respectively. Due to pump power limitations we studied MHz repetition rates separately for 1 MHz and 2 MHz. As shown in

Fig. 4.6(b), with increasing pump pulse repetition rate from 1 MHz to 2 MHz by preserving pump peak power ultra-broad supercontinuum could be reproduced.

With 2 MHz pump pulse repetition rate, we measured 3.96 W and 3.50 W average output powers for supercontinua generated in 10 m and 20 m GIMF, respectively. The launched pump power in this measurements is 4.62 W. For 20 m propagation length more broad supercontinuum generation is feasible but this also causes reduction in output average power. Our results indicate that by increasing average power and repetition rate simultaneously, higher average powers can be obtained with standard GIMF to acquire octave-spanning supercontinuum. Moreover we performed supercontinuum studies with 20 m GIMF with 50 μm core diameter to investigate the effect of core size on supercontinuum generation. Even though self-imaging periods are different for 50 μm and 62.5 μm core diameters, similar cascaded Raman scattering and supercontinuum evolution also observed in graded-index MMF with 50 μm core diameter. The spectral difference is presented in Fig. 4.6(c) with both fibers with 1 MHz repetition rate and same average output power. The generated supercontinuum features similar spectrum with the results obtained via 62.5 μm core diameter.

4.3 Numerical Results

To understand supercontinuum generation in GIMFs we numerically studied the evolution formation. For relatively long test fiber, we preferred the model based on 1+1D generalized nonlinear Schrödinger equation (Eq.2.21) with a periodic nonlinear coefficient $\gamma(z)$ to imitate spatiotemporal beam propagation inside the graded-index MMFs. This model is explained in the Chapter 2 with more details.

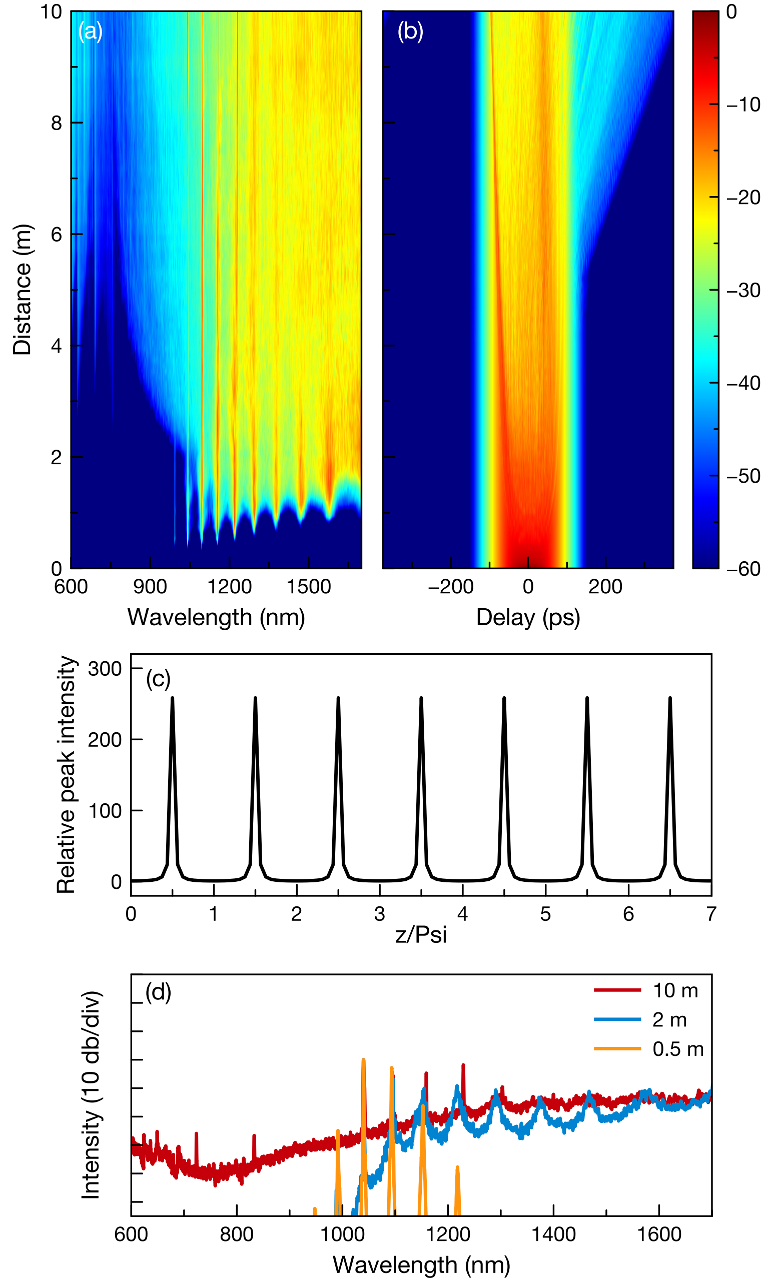

Figure 4.7: Results obtained by averaging of numerical simulations showing (a) spectral and (b) temporal evolution through 10 m graded-index MMF with 62.5 μm core diameter. (c) Relative peak intensity imposed by nonlinear coefficient in simulations. Self-imaging period Psi = 503.6 μm. (d) Numerically obtained spectral evolution for different propagation lengths.

Obtained numerical results are presented in Fig. 4.7(a,b) and feauteres spectral and temporal evolution in 10 m GIMF with 62.5 μm core diameter. In simulations, 70 ps duration with 30 kW peak power is defined for pump pulses centered at 1040 nm. We employed the the fourth-order Runge-Kutta in the Interaction Picture method for high accuracy in numerical calculations [28, 61]. We defined beam spot size at the fiber facet (a_0) as 20μm, n_2 as $3.2x10^{-20}m^2/W$, relative index difference as 0.019, time window width as 750 ps with 2 fs resolution. In simulations, Raman process (f_R), shock terms and high-order dispersion coefficients up to β_7 are considered. SRS is included in the equation via use of a response function [22]. To simulate experimental observations more accurately we averaged the simulations over 4 set of initial conditions. The considered relative peak intensity with the aforementioned parameters is presented in Fig. 4.7(c). The integration step in simulations is defined as 125.91μm to avoid aliasing in periodic nonlinearity term.

Results after propagating 50 cm, 2 m and 10 m is presented to demonstrate spectral broadening and wavelength conversion. We noticed that generation of new wavelengths at anomalous dispersion resembles development of Raman soliton components [62]. This formation ensures spectral flatness in supercontinuum generation. These soliton dynamics cause to temporal breakup observed in the simulations after 5 m propagation. Numerically obtained supercontinuum spectrum features similar behavior with the experimental results even though loss terms are not included.

4.4 Conclusion

To conclude, in this chapter we presented a novel approach to generate watt-level octave-spanning spectral flat supercontinua based on unique cascaded Raman scattering effect in a GIMF. State of the art results for GIMF ($\sim$ 4 W) are achieved with 62.5 μm core diameter using picosecond pulses at MHz repetition rate. Our results presents unique cascaded SRS observed in GIMF plays a crucial role in the supercontinuum evolution. For different wavelength ranges spatial distribution of the generated supercontinua features Gaussian-like beam shapes. Our results shown that this low-cost graded-index multimode fiber-based supercontinuum source could exploit the multimode features of GIMF to reach high power level average powers.

Chapter 5

All-fiber Lasers with Multimode Interference-based Saturable Absorber

5.1 Introduction

Fiber laser systems are commonly used in various applications such as medical applications, metrology and material processing [63]. By featuring high and broadband gain the ytterbium based fiber laser systems are mainly preffered in photonic systems. Over the years different mode-locking techniques are proposed to generate ultrashort pulses with a ytterbium based fiber laser solution. Soliton, dissipative soliton and self-similar pulses are studied extensivly with this motivation in the fiber oscillator field [64, 55, 10, 8]. To achieve stable mode-locking operation with these lasers a dispersion mapping is required inside the laser cavity. Since the 1μm range is at the normal dispersion of the standard optical fibers dispersion mapping requires bulk optics such as gratings and structured fibers. These additional segments increases the complexity of the fiber laser and fiber-based cavity losses its compactness. A stable passivly mode-locked all-normal dispersion fiber laser is demonstrated in 2006 by Chong at al. [9]. In this cavity design the internal pulse evolution is strongly depends on bandpass filtering of the chirped pulses. Researchers extensively studied the dynamics of all-normal dispersion fiber laser and its pulse type dissipative solitons over the years [39]. The power and energy handling capacity of the dissipative solitons are demonstrated with very-large-mode-area- fiber [40, 11]. On the other hand, all-fiber dissipative soliton lasers are a subject of high interest owing to their compact and misalignment free designs. Researchers presented various methods to obtain all-fiber dissipative soliton lasers with different in-line bandpass filter designs [65, 66, 67, 68]. For achieve mode-locking nonlinear polarization evolution (NPE) and material based saturable absorbers are generally preferred in these studies.

Additional to featuring various spatiotemporal nonlinear dynamics, possibility of saturable absorber dynamics of a short GIMF segment is studied theoretically by Nazemosadat et al. [69]. They proposed a device design based on nonlinear multimodal interference (NL-MMI) to achieve saturable absorber attribute from a GIMF segment in between single mode fiber segments. The calculations of Nazemosadat et al. show that 90% modulation depth is possible for a saturable absorber based on their design. On the other hand, Mohammed et al. proposed a similar design to construct an all-fiber bandpass filter and studied both numerically and experimentally [70]. Their proposed design exploits the multimode interference reimaging phenomenon to work as a filter. Later, Mafi et al. presented a low-loss wavelength dependent coupler structure by implementing a graded-index multimode fiber segment to this filter structure [71]. The first experimental verification of GIMF based saturable absorber is demonstrated very recently with a thulium based all-fiber soliton oscillator structure [72]. Li et al. slightly modified the Nazemosadat et al.'s design by placing a step-index multimode fiber before the GIMF to achieve better excitation. They demonstrated a soliton all-fiber oscillator capable to generate 1.4 ps pulses at 1888 nm with 19.82 MHz repetition rate and 0.6 mW output average powers. The proposed NL-MMI based saturable absorber configuration also supports bandpass filter structure thus it is very promising for all-normal dispersion lasers to obtain dissipative soliton pulses with simple and all-fiber cavity design. However, to the best of our knowledge, there are no reports on benefitting these effects to achieve all-fiber all-normal dispersion laser which capable to generate dissipative soliton pulses.

In this chapter we demonstrated the first all-fiber integrated all-normal dispersion Yb-doped oscillator with NL-MMI based saturable absorber capable to generate ultrashort pulses both numerically and experimentally. Our proposed simple cavity is a low-cost and compact solution to generate dissipative soliton fiber laser. We first performed numerical simulations to investigate the mode-locking dynamics and the promising results are lead us to experimental studies. Experimentally we obtained self-starting fundamental mode-locking with our all-fiber cavity design which dissipative solitons at 1030 nm with 5.8 mW average power and 44.25 MHz repetition rate. Chirped dissipative soliton pulses are compressed externally to 276 fs.

5.2 Numerical Results

Our proposed oscillator scheme is presented in the Fig. 5.1. We prefered to use the step-index multimode fiber (105/125) to GIMF (62.5/125) configuration as described by Li et al. [72] to sufficiently excite the GIMF. The length of the multimode fibers used in saturable absorber segment is important for mode-locking threshold and bandwidth of the bandpass filter. We determined the GIMF length as 14 cm to achieve $\sim$ 15 nm bandwidth for multimode interference based bandpass filtering based on the calculations of Mohammed et al. and Mafi et al. [70, 71]. With 0.5 cm step-index multimode fiber segment, the total length of the NL-MMI based saturable absorber segment is defined as 14.5 cm. Theoretical studies suggest that the transmission behavior of NL-MMI based saturable absorber has a sinusoidal behavior [69]. According to these studies or a constant fiber length, one can achieve desired modulation depth with optimum GIMF length and energy splitting between the modes.

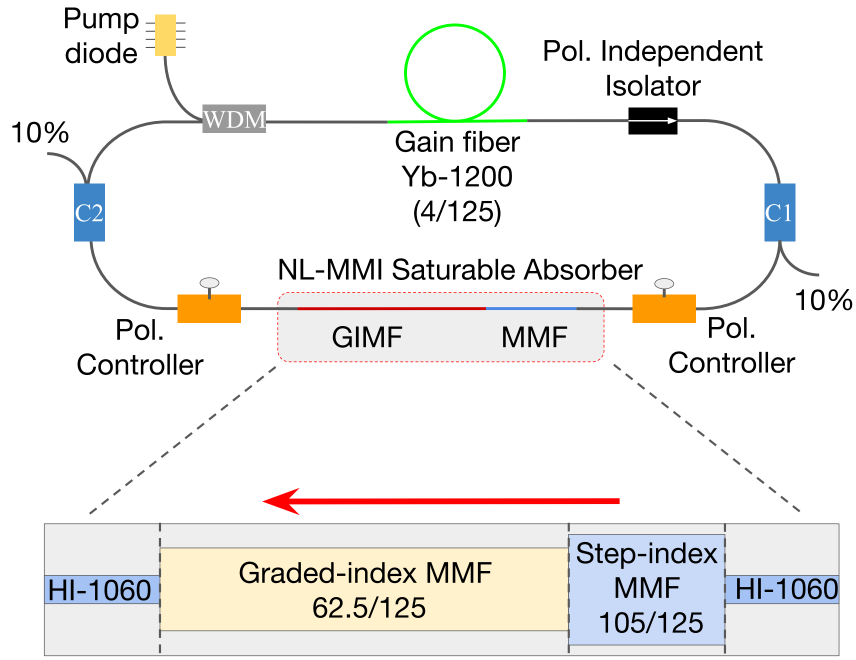

Figure 5.1: Schematic of the all-fiber Yb-doped laser with NL-MMI based saturable absorber: WDM, wavelength division multiplexer; GIMF, graded-index multimode fiber; MMF, multimode fiber.

Based on the model described in [1, 73, 61], we performed numerical simulations to investigate possibility of mode-locking with the fiber laser cavity presented in Fig. 5.1. We modeled the saturable absorber behavior of the GIMF device with the following transfer function,

$$T = q_0 + q_1 sin^2(I/I_{sat}) \tag{5.1}$$

where $q_0 = 0.15$ is the minimum transmission, $q_1 = 0.85$ is the modulation depth, I is instantaneous pulse power and $I_{sat} = 0.4$nJ is the saturation power [69]. We considered the the energy in the higher order modes remained after the propagating GIMF as an additional intracavity loss. Thus in the simulations, we only consider pulse propagation in the fundamental mode and introduce an additional loss term at the saturable absorber segment. By simply comparing the mode areas of the single mode fiber and GIMF we consider this loss term os 0.95 in our simulations. As we calculated according the model of Mafi et al. [71],

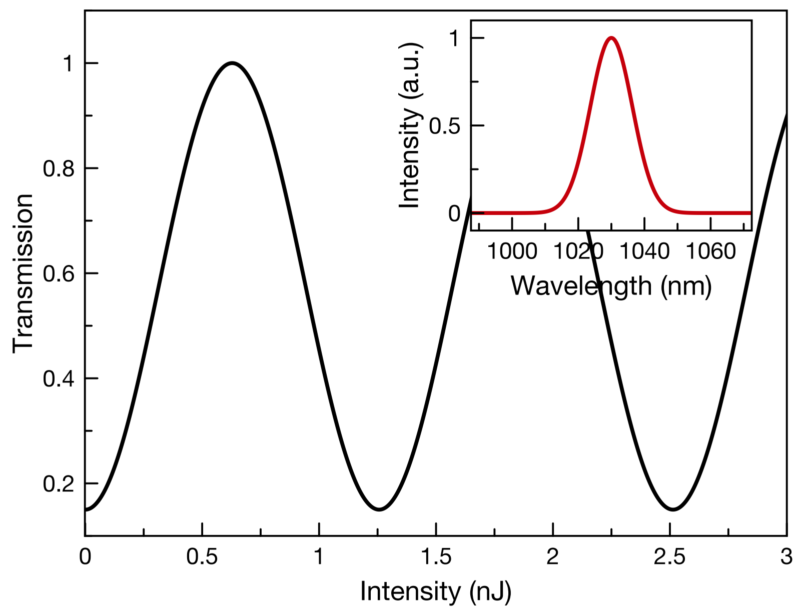

Figure 5.2: Transmission of the GIMF saturable absorber considered in numerical studies. Inset: Transmission spectrum of the bandpass filter considered in numerical studies.

additional to saturable absorber behavior to GIMF segment we add bandpass filter property with 15 nm bandwidth to our simulations. We included Raman and shock terms in our simulations and implement gain profile of the ytterbium active fiber segment as Lorentzian with 40 nm bandwidth and 30 dB small-signal gain.

Numerical simulations are performed according to fourth-order Runge-Kutta in the interaction picture method [28, 61]. From quantum noise a stable mode-lock operation is achieved and demonstrated in Fig. 5.3. The evolution of the pulse inside the oscillator is presented in temporal and spectral domains (Fig. 5.3(a)). Our results shows that gain filtering in the first part of the active fiber and spectral broadening in the following fiber segments. Filtering and chirping based pulse shaping is achieved with implemented bandpass filter. Self-consistent dissipative soliton pulse formation is ensured with strong amplification factor of the ytterbium fiber segment even though intracavity loss is assumed relatively high. Obtained spectra for output couplers before and after the gain fiber are

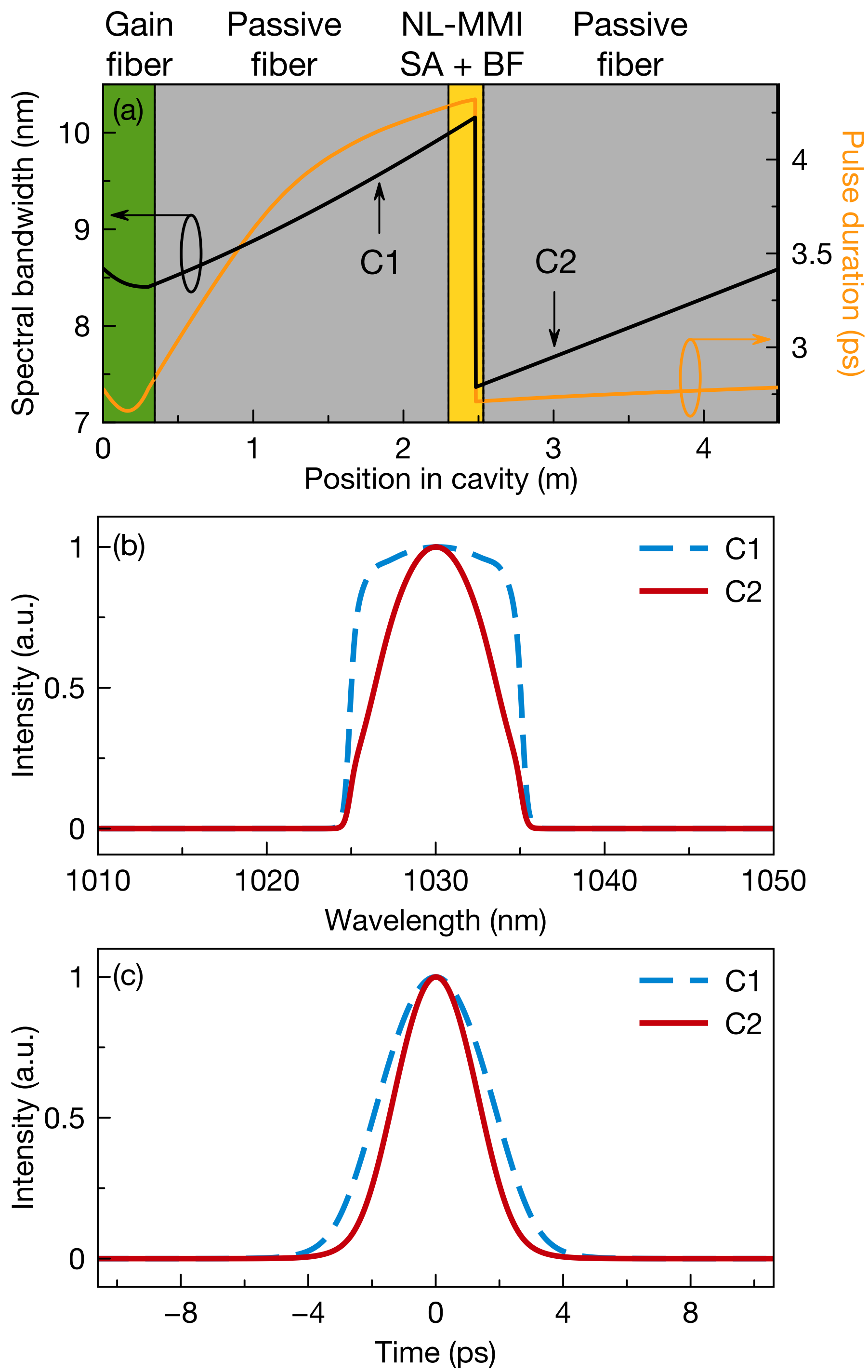

Figure 5.3: (a) Simulated pulse duration and spectral bandwidth variation over the cavity: SA, saturable absorber; BF, bandpass filter. (b) Simulated laser spectra obtained from the defined output couplers. C1 (C2) is defined after (before) the gain fiber segment. (c) Simulated temporal profile obtained at the output couplers C1 and C2.

have 10 nm and 7.3 nm bandwidths respectively (Fig. 5.3(b)). As presented in Fig. 5.3(c), the output pulse duration of 3.9 ps and 2.9 ps obtained respectively for these couplers.

5.3 Experimental Results

Encouraged with the simulation results, we experimentally constructed the same fiber laser cavity. The gain section of the oscillator is 30 cm highly doped ytterbium fiber (Yb-1200-4/125) pumped by 976 nm fiber-coupled diode laser. An inline polarization independent isolator is preferred to determine the propagation direction with eliminating the possibility of NPE mode-locking. Output couplers are preferred with 10% output rates as simulation suggests to investigate the effect of NL-MMI based saturable absorber segment. NL-MMI saturable absorber segment is developed by 0.5 cm step-index multimode fiber with 105 μm core and 125 μm cladding diameter (Nufern MM-S105/125) and 14 cm graded-index multimode fiber with 62.5 μm core and 125 μm cladding diameter (Thorlabs GIF625). The required intra-cavity brifiringence to actiheve mode-locking is obtained with fiber polarization controllers.

At 400 mW pump power, self-starting fundamental mode-locking is obtained with ~44 MHz repetition rate. Spectral measurements are performed from the couplers placed before and after the GIMF saturable absorber segment and presented in Fig. 5.4(a). Spectral bandwidths are recorded as 11.8 nm and 11.4 nm at -7 dB from the couplers C1 and C2, respectively. From the same output ports the output power of the laser is measured as 5.8 mW and 0.15 mW, respectively. As the he numerical simulations predicted, the intra-cavity pulse energy of 1.3 nJ obtained experimentally before the output coupler (C1). The laser produces chirped pulses with $\sim$ 5 ps duration (from C1 output coupler) as presented in the autocorrelation trace in Fig. 5.4(b). Using an external grating pair with 300 line/mm we compressed these pulses. As demonstrated in Fig. 5.5(a), the minimum pulse duration of 276 fs is obtained with Gaussian deconvolution factor. We used PICASO algorithm to retrieve temporal profile of the compressed pulses

[74]. The PICASO-retrieved shape of the pulse is presented in the Fig. 5.5(b). With PICASO algorithm, the retrieved pulse duration is calculated as 236 fs.

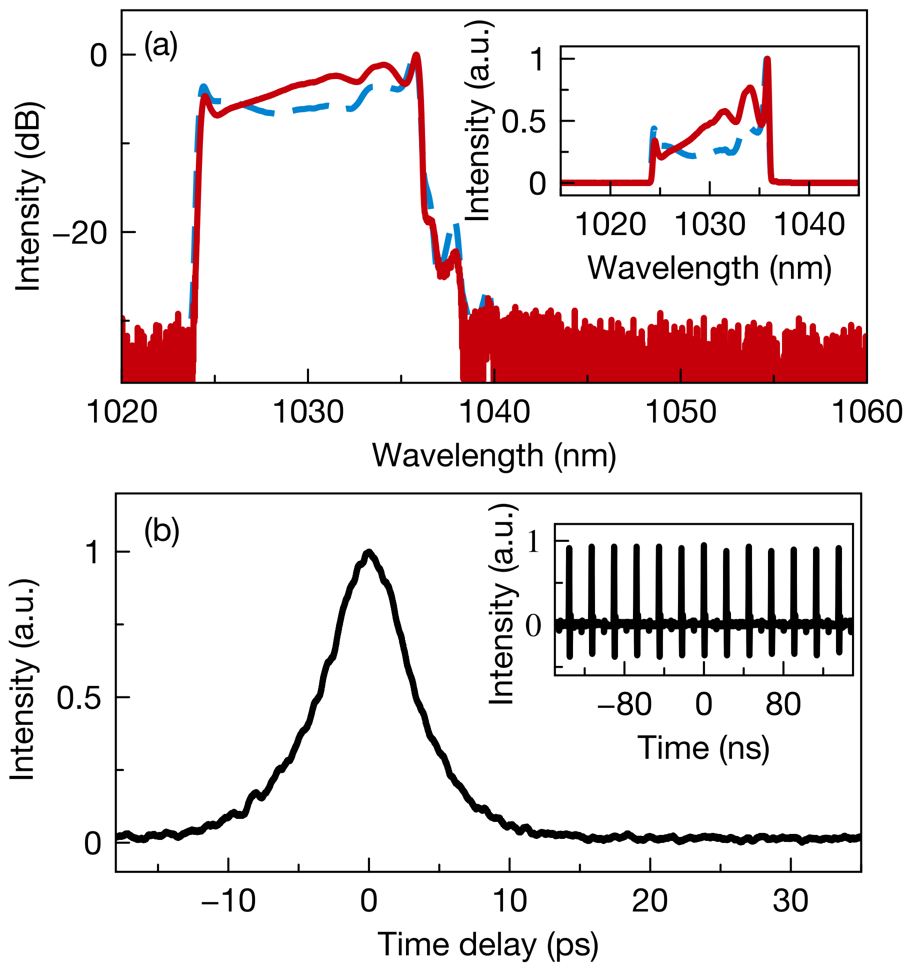

Figure 5.4: Spectra of dissipative soliton pulse from the output couplers on logarithmic (a) and linear scale (inset). Measurements from C1 and C2 couplers are indicated as blue and red, respectively. (b) Autocorrelations trace of the chirped pulses obtained directly from output coupler C1. Inset: Single-pulse train.

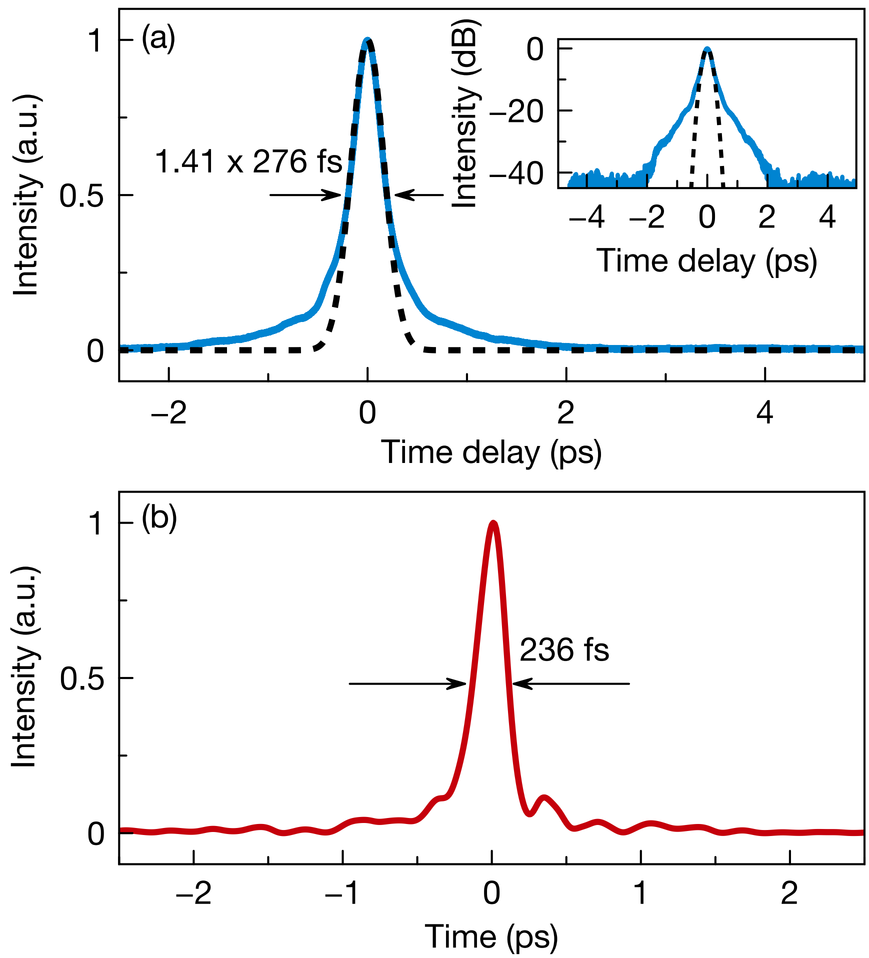

Figure 5.5: (a) Autocorrelation trace of the dechirped pulses obtained from output coupler C1 (solid) and theoretical fit with Gaussian pulse shape (dashed). Inset: In logarithmic scale. (b) PICASO retrieved dechirped pulse shape.

We characterized our novel all-fiber mode-lock laser cavity in the frequency domain as well. With a with radio frequency (RF) analyzer, the fundamental repetition rate of the laser is measured as 44.25 MHz. We recorded the RF spectrum with 1 kHz span and 10 Hz resolution bandwidth and obtained sideband suppression ratio around 70 dB (Fig. 5.6). We measured RF spectrum with 1 GHz span and 3 kHz resolution bandwidth and our results indicates no periodic envelope or fluctuation observed in long-span. The fiber laser continues mode-locking operation uninterrupted for days and there is no sign of degradation.

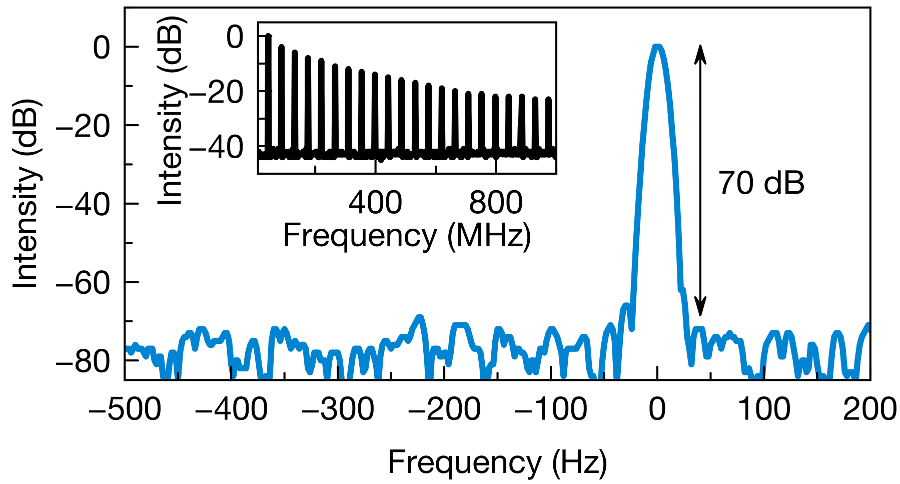

Figure 5.6: Measured RF spectrum with 1 kHz span and 10 Hz resolution bandwidth, with central frequency shifted to zero for clarity. Inset, RF spectrum with 1 GHz span and 3 kHz resolution bandwidth.

5.4 Conclusion

To summarize, we demonstrated an all-fiber all-normal dispersion ytterbium-doped oscillator with nonlinear multimodal interference based saturable absorber capable both numerically and experimentally, first time in the literature. The presented laser cavity generates ultrashort dissipative soliton pulses with an all-fiber cavity design. All-fiber structure is ensured via multimode interference reimaging-based saturable absorber and bandpass filtering with employing a small GIMF segment. The demonstrated laser cavity is an alternative approach to generate dissipative soliton mode-locking with the low-cost and simple design. The oscillator generates dissipative soliton pulses at 1030 nm with 5.8 mW average power, 0.13 nJ energy, 5 ps duration and 44.25 MHz repetition rate. Via an external grating pair, pulses are dechirped to 276 fs. Since all-fiber cavity desing ensures high stability, ∼70 dB sideband suppression is recorded in RF spectrum.

Chapter 6

Conclusion and Outlook

In this thesis, we extensively studied spatiotemporal nonlinear dynamics in multimode fibers with a graded-index refractive profile. In Chapter 3, we investigate the spatiotemporal propagation of femtosecond pulses. Our results demonstrated spatiotemporal instability phenomenon with 200 fs pump pulses first time in the literature. Instability sidebands are recorded with 91 THz frequency shift from the pump wavelength. Numerical studies are performed to investigate nature of the femtosecond spatiotemporal instability. Our studies verify the recently presented universal attractor model. With intrinsically large frequency shift, we believe spatiotemporal instability of femtosecond sidebands can be used to generate desired wavelengths for various applications such as imaging and microscopy.

In Chapter 4, we presented a novel technique to generate multi-watt-level octave-spanning supercontinuum triggered by cascaded-Raman scattering for the first time. We developed a home-made high power fiber laser system to study picosecond nonlinear pulse propagation in GIMFs. Our studies revealed that unique cascaded-Raman scattering effect can lead to supercontinuum formation in the normal dispersion. We exploited this dynamic and achieve spectrally flat octave-spanning $\sim$4 W average output with 2 MHz pump repetition rate.The obtained results are the highest average power and repetition rate supercontinuum source ever generated with standard GIMF. We demonstrated a low-cost method to generate watt-level supercontinua with Gaussian-like beam profiles. For biomedical systems and measurement methods with our proposed approach multimode fibers can offer higher average power with MHz repetition rates due to the power handling capacity.

Finally, in Chapter 5, we demonstrated an innovative approach to generate dissipative soliton pulses from an all-fiber oscillator by employing a short GIMF segment. Saturable absorption and spectral band-pass filtering are ensured via multimode interference in GIMF fiber. With these functionalities, all-normal dispersion all-fiber mode-locked laser is introduced the first time in the literature.The proposed cavity is studied experimentally and numerically. Dissipative soliton pulses with few picosecond duration are obtained from the all-fiber oscillator and dechirped to 276 fs externally. In RF measurements, all-fiber cavity design features 70 dB sideband suppression. We believe our proposed cavity design is a low-cost and simple approach to generate dissipative soliton pulses from an all-fiber laser structure and can be power scaled with large-mode-area fibers and photonics crystal fibers.

Bibliography

[1] G. P. Agrawal, *Nonlinear fiber optics.* Academic press, 2007.

[2] D. Colladon, "On the reflections of a ray of light inside a parabolic liquid stream," *Comptes Rendus*, vol. 15, pp. 800–802, 1842.

[3] K. Kao and G. A. Hockham, "Dielectric-fibre surface waveguides for optical frequencies," in *Proceedings of the Institution of Electrical Engineers*, vol. 113, pp. 1151–1158, IET, 1966.

[4] R. J. Mears, L. Reekie, I. Jauncey, and D. N. Payne, "Low-noise erbium-doped fibre amplifier operating at 1.54 μm," *Electronics Letters*, vol. 23, no. 19, pp. 1026–1028, 1987.

[5] I. Alcock, A. Ferguson, D. Hanna, and A. Tropper, "Mode-locking of a neodymium-doped monomode fibre laser," *Electronics Letters*, vol. 22, no. 5, pp. 268–269, 1986.

[6] J. Kafka, T. Baer, and D. W. Hall, "Mode-locked erbium-doped fiber laser with soliton pulse shaping," *Optics letters*, vol. 14, no. 22, pp. 1269–1271, 1989.

[7] M. Fermann, V. Kruglov, B. Thomsen, J. Dudley, and J. Harvey, "Self-similar propagation and amplification of parabolic pulses in optical fibers," *Physical Review Letters*, vol. 84, no. 26, p. 6010, 2000.

[8] F. Ilday, J. Buckley, W. Clark, and F. Wise, "Self-similar evolution of parabolic pulses in a laser," *Physical review letters*, vol. 92, no. 21, p. 213902, 2004.

[9] A. Chong, J. Buckley, W. Renninger, and F. Wise, "All-normal-dispersion femtosecond fiber laser," *Optics Express*, vol. 14, no. 21, pp. 10095–10100, 2006.

[10] J. Dudley, A. Peacock, V. Kruglov, B. Thomsen, J. Harvey, M. Fermann, G. Sucha, and D. Harter, "Generation and interaction of parabolic pulses in high gain fiber amplifiers and oscillators," in *Optical Fiber Communication Conference*, p. WP4, Optical Society of America, 2001.

[11] M. Baumgartl, C. Lecaplain, A. Hideur, J. Limpert, and A. Tünnermann, "66 w average power from a microjoule-class sub-100 fs fiber oscillator," *Optics letters*, vol. 37, no. 10, pp. 1640–1642, 2012.

[12] H. Pourbeyram, G. P. Agrawal, and A. Mafi, "Stimulated raman scattering cascade spanning the wavelength range of 523 to 1750 nm using a graded-index multimode optical fiber," *Applied Physics Letters*, vol. 102, no. 20, p. 201107, 2013.

[13] W. H. Renninger and F. W. Wise, "Optical solitons in graded-index multimode fibres," *Nature communications*, vol. 4, p. 1719, 2013.

[14] K. Krupa, A. Tonello, B. M. Shalaby, M. Fabert, A. Barthélémy, G. Millot, S. Wabnitz, and V. Couderc, "Spatial beam self-cleaning in multimode fibres," *Nature Photonics*, vol. 11, pp. 237–241, mar 2017.

[15] G. Lopez-Galmiche, Z. S. Eznaveh, M. Eftekhar, J. A. Lopez, L. Wright, F. Wise, D. Christodoulides, and R. A. Correa, "Visible supercontinuum generation in a graded index multimode fiber pumped at 1064 nm," *Optics letters*, vol. 41, no. 11, pp. 2553–2556, 2016.

[16] K. Krupa, A. Tonello, A. Barthélémy, V. Couderc, B. M. Shalaby, A. Bendahmane, G. Millot, and S. Wabnitz, "Observation of geometric parametric instability induced by the periodic spatial self-imaging of multimode waves," *Physical review letters*, vol. 116, no. 18, p. 183901, 2016.

[17] L. G. Wright, S. Wabnitz, D. N. Christodoulides, and F. W. Wise, "Ultrabroadband dispersive radiation by spatiotemporal oscillation of multimode waves," *Physical review letters*, vol. 115, no. 22, p. 223902, 2015.

[18] U. Teğin and B. Ortaç, "Spatiotemporal instability of femtosecond pulses in graded-index multimode fibers," *IEEE Photonics Technology Letters*, vol. 29, no. 24, pp. 2195–2198, 2017.

[19] U. Teğin and B. Ortaç, "High power high repetition rate supercontinuum generation in graded-index multimode fibers," *arXiv preprint arXiv:1709.09158*, 2017.

[20] U. Teğin and B. Ortaç, "All-fiber all-normal-dispersion femtosecond laser with nonlinear multimodal interference based-saturable absorber," *Optics letters*, vol. 43, no. 7, pp. 1611–1614, 2018.

[21] I. Malitson, "Interspecimen comparison of the refractive index of fused silica," *Josa*, vol. 55, no. 10, pp. 1205–1209, 1965.

[22] R. H. Stolen, J. P. Gordon, W. Tomlinson, and H. A. Haus, "Raman response function of silica-core fibers," *JOSA B*, vol. 6, no. 6, pp. 1159–1166, 1989.

[23] E. Ippen and R. Stolen, "Stimulated brillouin scattering in optical fibers," *Applied Physics Letters*, vol. 21, no. 11, pp. 539–541, 1972.

[24] J. Kafka and T. Baer, "Fiber raman soliton laser pumped by a nd: Yag laser," *Optics letters*, vol. 12, no. 3, pp. 181–183, 1987.

[25] S. A. Babin, E. V. Podivilov, D. S. Kharenko, A. E. Bednyakova, M. P. Fedoruk, V. L. Kalashnikov, and A. Apolonski, "Multicolour nonlinearly bound chirped dissipative solitons," *Nature communications*, vol. 5, 2014.

[26] U. Tegin, P. Elahi, Ç. Şenel, E. Ergeçen, and F. Ö. Ilday, "Dissipative solitons generated from a mode-locked raman laser," in *The European Conference on Lasers and Electro-Optics*, p. CJ_2_6, Optical Society of America, 2015.

[27] J. M. Dudley and J. R. Taylor, *Supercontinuum generation in optical fibers*. Cambridge University Press, 2010.

[28] J. Hult, "A fourth-order runge–kutta in the interaction picture method for simulating supercontinuum generation in optical fibers," *Journal of Lightwave Technology*, vol. 25, no. 12, pp. 3770–3775, 2007.

[29] Z. Liu, L. G. Wright, D. N. Christodoulides, and F. W. Wise, "Kerr self-cleaning of femtosecond-pulsed beams in graded-index multimode fiber," *Optics Letters*, vol. 41, no. 16, pp. 3675–3678, 2016.

[30] L. G. Wright, Z. Liu, D. A. Nolan, M.-J. Li, D. N. Christodoulides, and F. W. Wise, "Self-organized instability in graded-index multimode fibres," *Nature Photonics*, vol. 10, p. 771, 2016.

[31] S. Raghavan and G. P. Agrawal, "Spatiotemporal solitons in inhomogeneous nonlinear media," *Optics Communications*, vol. 180, no. 4-6, pp. 377–382, 2000.

[32] F. Poletti and P. Horak, "Description of ultrashort pulse propagation in multimode optical fibers," *JOSA B*, vol. 25, no. 10, pp. 1645–1654, 2008.

[33] A. Mafi, "Pulse propagation in a short nonlinear graded-index multimode optical fiber," *Journal of Lightwave Technology*, vol. 30, no. 17, pp. 2803–2811, 2012.

[34] L. G. Wright, D. N. Christodoulides, and F. W. Wise, "Controllable spatiotemporal nonlinear effects in multimode fibres," *Nature Photonics*, vol. 9, no. 5, pp. 306–310, 2015.

[35] M. Conforti, C. M. Arabi, A. Mussot, and A. Kudlinski, "Fast and accurate modeling of nonlinear pulse propagation in graded-index multimode fibers," *Optics Letters*, vol. 42, no. 19, pp. 4004–4007, 2017.

[36] I. Duling, "Subpicosecond all-fibre erbium laser," *Electronics Letters*, vol. 27, no. 6, pp. 544–545, 1991.

[37] K. Tamura, E. Ippen, H. Haus, and L. Nelson, "77-fs pulse generation from a stretched-pulse mode-locked all-fiber ring laser," *Optics letters*, vol. 18, no. 13, pp. 1080–1082, 1993.

[38] F. Ö. Ilday, J. Buckley, L. Kuznetsova, and F. W. Wise, "Generation of 36-femtosecond pulses from a ytterbium fiber laser," *Optics Express*, vol. 11, no. 26, pp. 3550–3554, 2003.

[39] P. Grelu and N. Akhmediev, "Dissipative solitons for mode-locked lasers," *Nature photonics*, vol. 6, no. 2, p. 84, 2012.

[40] B. Ortaç, M. Baumgartl, J. Limpert, and A. Tünnermann, "Approaching microjoule-level pulse energy with mode-locked femtosecond fiber lasers," *Optics letters*, vol. 34, no. 10, pp. 1585–1587, 2009.

[41] N. Doran and D. Wood, "Nonlinear-optical loop mirror," *Optics Letters*, vol. 13, no. 1, pp. 56–58, 1988.

[42] M. E. Fermann, F. Haberl, M. Hofer, and H. Hochreiter, "Nonlinear amplifying loop mirror," *Optics Letters*, vol. 15, no. 13, pp. 752–754, 1990.

[43] J. Szczepanek, T. M. Kardaś, M. Michalska, C. Radzewicz, and Y. Stepanenko, "Simple all-pm-fiber laser mode-locked with a nonlinear loop mirror," *Optics letters*, vol. 40, no. 15, pp. 3500–3503, 2015.

[44] A. Martinez and Z. Sun, "Nanotube and graphene saturable absorbers for fibre lasers," *Nature Photonics*, vol. 7, no. 11, p. 842, 2013.

[45] U. Keller, K. J. Weingarten, F. X. Kartner, D. Kopf, B. Braun, I. D. Jung, R. Fluck, C. Honninger, N. Matuschek, and J. A. Der Au, "Semiconductor saturable absorber mirrors (sesam's) for femtosecond to nanosecond pulse generation in solid-state lasers," *IEEE Journal of selected topics in QUANTUM ELECTRONICS*, vol. 2, no. 3, pp. 435–453, 1996.

[46] B. Ortaç, M. Plötner, T. Schreiber, J. Limpert, and A. Tünnermann, "Experimental and numerical study of pulse dynamics in positive net-cavity dispersion mode-locked yb-doped fiber lasers," *Optics express*, vol. 15, no. 23, pp. 15595–15602, 2007.

[47] S. Longhi, "Modulational instability and space time dynamics in nonlinear parabolic-index optical fibers," *Optics letters*, vol. 28, no. 23, pp. 2363–2365, 2003.

[48] E. Nazemosadat, H. Pourbeyram, and A. Mafi, "Phase matching for spontaneous frequency conversion via four-wave mixing in graded-index multimode optical fibers," *JOSA B*, vol. 33, no. 2, pp. 144–150, 2016.

[49] P. Horak and F. Poletti, *Multimode nonlinear fibre optics: theory and applications*. InTech, 2012.

[50] J. T. Manassah, P. L. Baldeck, and R. Alfano, "Self-focusing and self-phase modulation in a parabolic graded-index optical fiber," *Optics letters*, vol. 13, no. 7, pp. 589–591, 1988.

[51] M. Karlsson, D. Anderson, and M. Desaix, "Dynamics of self-focusing and self-phase modulation in a parabolic index optical fiber," *Optics letters*, vol. 17, no. 1, pp. 22–24, 1992.

[52] R. R. Alfano, *The Supercontinuum Laser Source: The Ultimate White Light*. Springer, 2016.

[53] T. A. Birks, J. C. Knight, and P. S. J. Russell, "Endlessly single-mode photonic crystal fiber," *Optics letters*, vol. 22, no. 13, pp. 961–963, 1997.

[54] K. Krupa, C. Louot, V. Couderc, M. Fabert, R. Guenard, B. Shalaby, A. Tonello, D. Pagnoux, P. Leproux, A. Bendahmane, *et al.*, "Spatiotemporal characterization of supercontinuum extending from the visible to the mid-infrared in a multimode graded-index optical fiber," *Optics Letters*, vol. 41, no. 24, pp. 5785–5788, 2016.

[55] B. Ortaç, A. Hideur, T. Chartier, M. Brunel, C. Özkul, and F. Sanchez, "90-fs stretched-pulse ytterbium-doped double-clad fiber laser," *Optics letters*, vol. 28, no. 15, pp. 1305–1307, 2003.

[56] J. Demas, L. Rishoj, X. Liu, G. Prabhakar, and S. Ramachandran, "High-power, wavelength-tunable nir all-fiber lasers via intermodal four-wave mixing," in *CLEO: Applications and Technology*, pp. JTh5A–8, Optical Society of America, 2017.

[57] E. Golovchenko, P. V. Mamyshev, A. N. Pilipetskii, and E. Dianov, "Mutual influence of the parametric effects and stimulated raman scattering in optical fibers," *IEEE Journal of Quantum Electronics*, vol. 26, no. 10, pp. 1815–1820, 1990.

[58] F. Vanholsbeeck, P. Emplit, and S. Coen, "Complete experimental characterization of the influence of parametric four-wave mixing on stimulated raman gain," *Optics letters*, vol. 28, no. 20, pp. 1960–1962, 2003.

[59] S. Coen, D. A. Wardle, and J. D. Harvey, "Observation of non-phase-matched parametric amplification in resonant nonlinear optics," *Physical review letters*, vol. 89, no. 27, p. 273901, 2002.

[60] J. M. Dudley, G. Genty, and S. Coen, "Supercontinuum generation in photonic crystal fiber," *Reviews of modern physics*, vol. 78, no. 4, p. 1135, 2006.

[61] Ç. Şenel, "33 femtosecond yb-doped optical frequency comb for frequency metrology applications," Master's thesis, Bilkent University, 2013.

[62] E. Golovchenko, P. V. Mamyshev, A. Pilipetskii, and E. M. Dianov, "Numerical analysis of the raman spectrum evolution and soliton pulse generation in single-mode fibers," *JOSA B*, vol. 8, no. 8, pp. 1626–1632, 1991.

[63] M. E. Fermann and I. Hartl, "Ultrafast fibre lasers," *Nature photonics*, vol. 7, no. 11, pp. 868–874, 2013.

[64] A. Isomäki and O. G. Okhotnikov, "Femtosecond soliton mode-locked laser based on ytterbium-doped photonic bandgap fiber," *Optics express*, vol. 14, no. 20, pp. 9238–9243, 2006.

[65] K. Kieu and F. Wise, "All-fiber normal-dispersion femtosecond laser," *Optics express*, vol. 16, no. 15, pp. 11453–11458, 2008.

[66] M. Schultz, H. Karow, O. Prochnow, D. Wandt, U. Morgner, and D. Kracht, "All-fiber ytterbium femtosecond laser without dispersion compensation," *Optics express*, vol. 16, no. 24, pp. 19562–19567, 2008.

[67] K. Özgören and F. Ilday, "All-fiber all-normal dispersion laser with a fiber-based lyot filter," *Optics letters*, vol. 35, no. 8, pp. 1296–1298, 2010.

[68] L. Zhang, J. Hu, J. Wang, and Y. Feng, "Tunable all-fiber dissipative-soliton laser with a multimode interference filter," *Optics letters*, vol. 37, no. 18, pp. 3828–3830, 2012.

[69] E. Nazemosadat and A. Mafi, “Nonlinear multimodal interference and saturable absorption using a short graded-index multimode optical fiber,” *JOSA B*, vol. 30, no. 5, pp. 1357–1367, 2013.

[70] W. S. Mohammed, P. W. Smith, and X. Gu, “All-fiber multimode interference bandpass filter,” *Optics letters*, vol. 31, no. 17, pp. 2547–2549, 2006.

[71] A. Mafi, P. Hofmann, C. J. Salvin, and A. Schülzgen, “Low-loss coupling between two single-mode optical fibers with different mode-field diameters using a graded-index multimode optical fiber,” *Optics letters*, vol. 36, no. 18, pp. 3596–3598, 2011.

[72] H. Li, Z. Wang, C. Li, J. Zhang, and S. Xu, “Mode-locked tm fiber laser using smf-simf-gimf-smf fiber structure as a saturable absorber,” *Optics express*, vol. 25, no. 22, pp. 26546–26553, 2017.

[73] G. Agrawal, *Applications of nonlinear fiber optics*. Academic press, 2001.

[74] J. Nicholson, J. Jasapara, W. Rudolph, F. Omenetto, and A. Taylor, “Full-field characterization of femtosecond pulses by spectrum and cross-correlation measurements,” *Optics letters*, vol. 24, no. 23, pp. 1774–1776, 1999.

Appendix A

Graded Index Multimode Fiber Simulation with SSFM and Periodic Nonlinearity

```
import numpy as np
import time
import matplotlib.pyplot as plt
t00 = time.time()
t000 = time.asctime()
print t000

## Input pulse parametes
pulsewidth=7e-12          # Initial pulse duration (s)
en = 2e-9                 # Pulse energy (J)
peakpower=en/pulsewidth
lamd=1030e-9              # Central wavelength (m)

twidth = pulsewidth*10
tres = 3e-15
```

```
timesteps = np.ceil(twidth/tres)
t0=np.arange(-twidth/2,twidth/2,tres)
t = np.array(t0)
fs=1/(timesteps*tres)
c=299792458.          # Speed of light (m/s)
w0 = (2*np.pi*c)/lamd

a0 = 15e-6                  # beam spot radius at z = 0 (m)
rc = 25e-6                  # GRIN fiber core radius (m)
nco = 1.470
ncl = 1.457
delta = (np.square(nco)-np.square(ncl))/(2*np.square(nco))
g = (2*delta)/np.square(rc)
b0 = (w0*nco)/c
C = 1/(np.square(b0)*np.square(a0**2)*g)
Zsi = np.pi*rc/np.sqrt(2*delta)

flen = 0.1                      # Fiber length (m)
dz = Zsi/8
z = np.arange(0,flen ,dz)
a2 = np.square(a0)*(np.square(np.cos(np.sqrt(g)*z)) \
                +C*np.square(np.sin(np.sqrt(g)*z)))

## Fiber parameters
beta2 = 21.16e-27       # s^2/m
n2 = 3.2e-20                # m2/W
Aeff = 2*np.pi*a2         # area of propagation
gama = (w0*n2)/(c*Aeff)

freq=c/lamd+fs*np.linspace(-timesteps/2,timesteps/2, \
                num=timesteps, endpoint=True)
omegas = 2*np.pi*freq
```

```
omg = np.array(omegas-w0)
## Gaussian pulse
E0=np.sqrt(peakpower)*np.exp(-0.5*np.square(t/pulsewidth*1.665))
Spec0 = np.square(np.abs(np.fft.fftshift(np.fft.fft(E0))))

## Split-Step Fourier Method
disp = ((0+1j)/2)*beta2*(omg)**2
linop = np.exp(dz*disp)
E = np.array(E0)
index = 0
sumz = 0.0
while sumz<=flen:
    f_temp = np.fft.fft(E)
    E1 = np.fft.ifft(linop*f_temp)
    nonop = (0+1j)*gama[index]*np.abs(E1)**2
    E = np.exp(dz*nonop)*E1
    index = index+1
    sumz = sumz+dz
    if np.mod(index,50) == 0:
        print sumz

## Normalization
Spec = np.square(np.abs(np.fft.fftshift(np.fft.fft(E))))
Spec = Spec/np.max(Spec)
Spec0 = Spec0/np.max(Spec0)

E_pulse = np.square(np.abs(E))/np.max(np.square(np.abs(E)))
E_pulse0 = np.square(np.abs(E0))/np.max(np.square(np.abs(E0)))
## Unit conversion
t = t*1e+12
wavelength = (c/freq)*1e+9

#elapsed = time.time() - t00
```

```
#print "Duration of simulation:",elapsed
print flen
t000 = time.asctime()
print t000

plt.subplot(2,1,1)
plt.plot(t,E_pulse,'r-')
axes = plt.gca()
axes.set_xlim([-twidth*1e+12/2,twidth*1e+12/2])
axes.set_xlabel('time (ps)')
axes.set_ylabel('Amplitude')
plt.subplot(2,1,2)
plt.semilogy(wavelength, abs(Spec), 'r-')
axes = plt.gca()
axes.set_xlabel('Wavelength (nm)')
axes.set_ylabel('Amplitude')
plt.show()
```